



Journal of
**Renewable Energy and Sustainable
Development**

RES**D**



Academy Publishing Center

Journal of Renewable Energy and Sustainable Development (RES D)

First edition 2015

© All rights reserved Copyright 2015

Permissions may be sought directly Academy Publishing Center,
Arab Academy for Science, Technology, and Maritime Transport,
Abu Kir Campus, Alexandria, EGYPT

P.O. Box: Miami 1029

Tel: (+203) 5622366/88 – EXT 1069 and (+203) 561 1818

Fax: (+203) 561 1818

Web Site: <http://apc.aast.edu>

No responsibility is assumed by the publisher for any injury and/or damage to persons or property as a matter of products liability, negligence or otherwise, or from any use or operation of any methods, products, instructions or ideas contained in the material herein.

Every effort has been made to trace the permission holders of figures and in obtaining permissions where necessary.

Volume 5, Issue 1, June 2019

ISSN: 2356-8518 Print Version

ISSN: 2356-8569 Online Version



Journal of Renewable Energy and Sustainable Development

RESD



Renewable Energy and Sustainable Development (RESD) is a biannual international peer-reviewed journal which presents a global forum for dissemination of research articles, case studies and reviews focusing on all aspects of renewable energy and its role in sustainable development. The topics of focal interest to RESD include, but are not limited to, all aspects of wind energy, wave/tidal energy, solar energy, as well as energy from biomass and biofuel. The integration of renewable energy technologies in electrical power networks and smart grids is another topic of interest to RESD. Experimental, computational and theoretical studies are all welcomed to RESD.

Sustainable development is a multidisciplinary advancing to the center of energy research with the declaration of UN millennium development goals for the first time in 2000, and continued to constitute a challenge in energy technologies in the past decade. RESD is mainly interested in case studies of sustainable development and its relation to transition economies in the Middle East, Africa, Asia and Oceania.

RESD has an outstanding editorial board of eminent scientists, researchers and engineers who contribute and enrich the journal with their vast experience in different fields of interest to the journal. The journal is open-access with a liberal Creative Commons Attribution-Non Commercial-4.0 International License. Which preserves the copyrights of published materials to the authors and protects it from unauthorized commercial use or derivation. The journal is financially supported by Arab Academy for Science, Technology and Maritime Transporting in order to maintain quality open-access source of research papers on renewable energy and sustainable development.

Editorial Committee



Editor-in-Chief

Yasser Gaber Dessouky, Ph.D

Professor of Electrical Engineering and Renewable Energy Technologies
Arab Academy for Science and Technology and Maritime Transport
(AASTMT) Abu Kir Campus, POBox: 1029 Miami,
Alexandria, EGYPT
E-mail: ygd@aast.edu

Associate Editors

Rania El Sayed Abdel Galil, Ph.D.

Associate Professor, Architectural Engineering and Environmental Design
Arab Academy for Science and Technology and Maritime Transport
(AASTMT) Abu Kir Campus, POBox: 1029 Miami,
Alexandria, EGYPT
Email: rania@aast.edu

Jingzheng Ren, Ph.D.

Associate Professor, Chemical Engineering
University of Southern Denmark,
DENMARK
Email: jire@iti.sdu.dk

Aly Ismail Shehata , Ph.D.

Assistant Professor, Mechanical Engineering
Arab Academy for Science and Technology and Maritime Transport
(AASTMT) Abu Kir Campus, POBox: 1029 Miami,
Alexandria, EGYPT
Email: aliismail@aast.edu

Ahmed Aboushady, Ph.D.

Assistant Professor, Electrical Engineering
Robert Gordon University,
Aberdeen, United Kingdom
a.aboushady@rgu.ac.uk

Editorial Board

Abdel Salam Hamdy Makhlouf, PhD

Professor, University of Texas – Pan American, USA

Adam Fenech, PhD

Associate Professor, University of Prince Albert Island, CANADA

Adel Al Taweel, PhD

Professor, Dalhousie University, CANADA

Ahmed Zobaa, PhD

Senior Lecturer, Brunel University London, U.K

Aziz Naamane, PhD

Senior Researcher, Laboratoire des Sciences de l'information et des Systèmes, FRANCE

Barry Wayne Williams, Ph.D

Professor, Strathclyde University, U.K

Chin-Hsiang Cheng, Ph.D

Professor, National Cheng Kung University, TAIWAN

Dieter Schramm, PhD

Professor, University of Duisburg-Essen, GERMANY

Ehab Fahmy El-Saadany, Ph.D

Professor, University of Waterloo, CANADA

Fei GAO, PhD

Associate Professor, University of Technology of Belfort-Montbéliard, FRANCE

Francesco Martinico, PhD

Professor, Università di Catania, ITALY

Frede Blaabjerg, PhD

Professor, Allborg University, DENMARK

Fouad H. Fouad, PhD

Professor, University of Alabama at Birmingham, U.S.A

Han-Seung Lee, PhD

Professor, Hanyang University, SOUTH KOREA

Hassan M.K. Abdel-Salam, PhD

Professor, Alexandria University, EGYPT

Hebatalla F. Abouelfadl, PhD

Associate Professor, Faculty of Fine Arts, Alexandria University, EGYPT

Jawad Faiz, Ph.D

Professor, University of Tehran, IRAN

Kouzou Abdellah, PhD

Associate Professor, Djelfa University, ALGERIA

Mohamed Youssef, PhD

Assistant Professor, University of Ontario, Institute of Technology, CANADA

Mohamed Ismail, PhD

Professor, Hanyang University, SOUTH KOREA

Moustafa Abdel-Maksoud, Dr.-Ing

Professor, Hamburg University of Technology, GERMANY

Nacer Msridi, PhD

Senior Researcher, Laboratoire des Sciences de l'information et des Systèmes, FRANCE

Pertter Breuhaus, PhD

Chief Scientist, International Research Institute Stavanger, NORWAY

Ping Zheng, PhD

Professor, Harbin Institute of Technology, CHINA

Robert F. Boehm, PhD

Professor, University of Nevada, Las Vegas, U.S.A

Robert W. Peters, Ph.D

Professor, University of Alabama, U.S.A

Sheldon Williamson, PhD

Associate Professor, University of Ontario, Institute of Technology, CANADA

Stephen Connelly, PhD

Senior Lecturer, the University of Sheffield, U.K

Suk Won Cha, PhD

Professor, Seoul National University, SOUTH KOREA

Susan Roaf, PhD

Professor, Heriot Watt University, U.K

Waleed F. Faris, PhD

Professor, International Islamic University of Malaysia, MALAYSIA

Yi-Tung Chen, Ph.D

Professor, University of Nevada Las Vegas, U.S.A

Youcef Soufi, PhD

Professor, University of Tébessa, ALGERIA

Advisory Board

Abbas Abdel Halim Yehia, PhD

Professor, Architectural Engineering & Environmental Design, Arab Academy for Science & Technology and Maritime Transport, Egypt

Abdel-Wahab Shalaby Kassem, PhD

Professor, Agricultural Engineering Department, Faculty of Agriculture, Alexandria University, Egypt

Adel Khalil, PhD

Professor, Mechanical Power Engineering Department Faculty of Engineering, Cairo University, Egypt

Ahmed Abu Saud, M.Sc

Chief Executive Officer (CEO) Of Egyptian Environmental Affairs Agency (EEAA)

Ahmed Hossam El-Din, PhD

Professor, Electrical Engineering Department, Alexandria University, Egypt

Almoataz Y. Abdelaziz, PhD

Professor, Faculty of Engineering, Ain Shams University, EGYPT

Amr A. Amin, PhD

Professor, Electric Power And Machines Department, Faculty of Engineering, Helwan University, Egypt

Anhar Ibrahim Hegazi, PhD

Director, Energy Efficiency Unit, IDSC, Egyptian Cabinet of Ministers, Egypt

Fatma Ahmed Moustafa Ali, PhD

Chairman for The Executive Committee for The Regional Center for Renewable Energy and Energy Efficiency (RCREEE), Egypt

Fatma El Zahraa Hanafi Ashour, PhD

Chairman, Chemical Engineering Department, Faculty of Engineering, Cairo University, Egypt

Fuad Ahmed Abulfotuh, PhD

Professor Emeritus, Alexandria University, Egypt

Galal Osman, PhD

Vice President, World Wind Energy Association (WWEA), Bonn, Germany

Hend Farouh, PhD

Executive Director of Central Unit For Sustainable Cities & Renewable Energy, New Urban Communities Authority, NUCA

Khaled El Zahaby, PhD

Chairman, Housing And Building National Research Center, HBRC, Cairo, Egypt

Mohamed Mostafa El-Khayat, PhD

Managing Director of Technical Affairs Sector, New And Renewable Energy Authority, Egypt

Mohamed Orabi, PhD

Director, Aswan Power Electronics Applications Research Center (APEARC), Aswan University, Egypt

Radwan H. Abdel Hamid, PhD

Professor, Helwan University, Egypt

Mohamed El Sobki

Executive Director, New And Renewable Energy Authority, Egypt

Tareq Emtairah, PhD

Executive Director, Regional Center for Renewable Energy and Energy Efficiency (RCREEE), Egypt

Peer Review Process

Peer review is an objective process at the heart of good scholarly publishing and is carried out on all reputable scientific journals. Our referees therefore play a vital role in maintaining the high standards of Renewable Energy and Sustainable Development (RESD) and all manuscripts are peer reviewed following the procedure outlined below.

Overall process for publishing a paper will be taken approximately 4 months after initial submission. Reviewing process will take about 2 months, and then publishing process will not exceed 2 months.

1. Initial manuscript evaluation

The Editor first evaluates all manuscripts. It is rare, but it is entirely feasible for an exceptional manuscript to be accepted at this stage. Those rejected at this stage are insufficiently original, have serious scientific flaws, have poor grammar or English language, or are outside the aims and scope of the journal. Those that meet the minimum criteria are passed on to at least 2 experts for review.

Authors of manuscripts rejected at this stage will normally be informed within 2 to 3 weeks of receipt.

2. Type of Peer Review

This journal employs single blind reviewing, the author identity is disclosed to the referee, while the referee remains anonymous throughout the process.

3. How the referee is selected

Referees are matched to the paper according to their expertise. Our database is constantly being updated. RESD has a policy of using single blind refereeing (as detailed in the previous section), with neither referee from the country of the submitting author. We welcome suggestions for referees from the author though these recommendations may or may not be used.

4. Referee reports

Referees are asked to evaluate whether the manuscript support followings key points related to scientific content, quality and presentation:

4.1. Technical

Scientific merit: notably scientific rigour, accuracy and correctness.

Clarity of expression; communication of ideas; readability and discussion of concepts.

Sufficient discussion of the context of the work, and suitable referencing.

4.2. Quality

Originality: Is the work relevant and novel?

Motivation: Does the problem considered have a sound motivation? All papers should clearly demonstrate the scientific interest of the results.

Repetition: Have significant parts of the manuscript already been published?

Length: Is the content of the work of sufficient scientific interest to justify its length?

4.3. Presentation

Title: Is it adequate and appropriate for the content of the article?

Abstract: Does it contain the essential information of the article? Is it complete? Is it suitable for inclusion by itself in an abstracting service?

Diagrams, figures, tables and captions: Are they essential and clear?

Text and mathematics: Are they brief but still clear? If you recommend shortening, please suggest what should be omitted.

Conclusion: Does the paper contain a carefully written conclusion, summarizing what has been learned and why it is interesting and useful?

Referees are not expected to correct or copyedit manuscripts. Language correction is not part of the peer review process.

5. How long does the review process take?

Typically the manuscript will be reviewed within 3 months. Should the referees' reports contradict one another or a report is unnecessarily delayed a further expert opinion will be sought. All our referees sign a conflict of interest statement. Revised manuscripts are usually returned to the initial referees within 1 week. Referees may request more than one revision of a manuscript.

6. Editorial decisions

After peer review and referee recommendation, the editor-in-chief, with the assistance of the associate editor, will study the paper together with reviewer comments to make one of the following decisions.

Accept

Accept pending minor revision: no external review required

Reject/Resubmit: major revisions needed and a new peer-review required

Reject

Digital Object Identifier

The RESD is supported by Digital Object Identifier, DOI for each article from Cross Ref.

The Code of the DOI of each article consists of the following format:

10.21622/RESD.YYYY.VV.I.PPP

Where

10.21622 = Journal Identifier

RESD = Journal name

YYYY = Four digits for the year

VV = Two digits for the Volume Number

I = One digit for the Issue Number

PPP = Three digits for the Number of the first page of the article

To look for the paper on line, search for this link
<http://dx.doi.org/10.21622/RESD.YYYY.VV.I.PPP>

Table of Contents

Editorials

Small Scale Renewable Generation Unlocking an Era of Peer-to-Peer Energy Trading and Internet of Energy

Ahmed Aboushady, Azmy I. Gowaid

1-2

Articles

The Challenges and Risks facing ICT in the Management and Operation of the Smart Grid

Tarek Mohammed Attia

3-14

Modelling and Energy Analysis of Solar Charging Facility for Electric Vehicles in Chile

Scarlett Allende

15-22

Voltage Clamping Circuits for Large Voltage Step-Down Coupled Inductor Converters

Richard Pollock

23-32

Site location and Pipeline routing optimization for Future natural gas importing terminal project in Morocco

Firdaous EL Ghazi, Mahmoud Akdi, Moulay Brahim Sedra

33-43

Small Scale Renewable Generation Unlocking an Era of Peer-to-Peer Energy Trading and Internet of Energy

*Dr. I A Gowaid and Dr. Ahmed Aboushady
Glasgow Caledonian University, 70 Cowcaddens Road,
Glasgow, G4 0BA, United Kingdom*

azmy.gowaid@gcu.ac.uk; ahmed.aboushady@gcu.ac.uk

Millions of people worldwide suffer from lack of reliable electric energy supply. Energy justice scholarship has noted that small scale decentralized renewable energy offers a unique opportunity to democratize local energy provision, increasing the access to and affordability of electricity for those who are currently on the margins of centralized energy provision systems. This, in turn, is believed to result in critical human development benefits at the local level.

There is a strong drive in the industrial and academic community toward the deregulation and decentralization of power systems to enable wider deployment of medium and small-scale renewable energy resources such as wind and solar systems. In a centralized power system, the flow of electric power is unidirectional from generators to consumers. In a decentralized system of distributed generators and consumers that are also able to produce energy (prosumers), power flow is no more unidirectional, and so are payments. To this end, peer-to-peer (P2P) energy trade concept aims to provide the business model and technical infrastructure enabling prosumers to trade their produced energy with one another in addition to (or instead of) trade with the utility. This eventually will realize a power grid structure based on the concept of Internet of Energy (IoE) where electric power becomes a commodity tradable in an open market. Implementation of this concept is made possible by the ongoing migration of traditional power grids from centralized systems to more decentralized networks so as to accommodate renewable and distributed energy resources (DERs) as well as Smart Grid infrastructure.

The generic P2P energy trading system can be represented as a four-layer architecture. The basic (physical) layer is the power grid layer followed by communications layer, a control layer, and business layer at the highest level. These interoperable layers control the whole P2P trading process whereas peers can be prosumers, electric vehicle (battery) owners, microgrids, or regions of the power system.

Much of the attention in the literature has been dedicated to developing appropriate structures of the communications and business layers in a bid to realize P2P trading without expensive alterations to the existing AC grid physical infrastructure. Therefore, researchers and innovators focus on developing platforms that run different forms of trading processes among peers taking in account grid security, economic incentives, and system operator requirements. Various criteria for peers to select who to trade with are possible, including 'least power loss', 'highest reliability' or 'most environmental'.

As it is very hard to trace actual power flows in a power grid and reward prosumers for their energy production, energy market regulators normally issue Renewable Energy Certificates (RECs) as an incentive for system operators to purchase renewable energy from DER owners. For instance, in the US each DER owner is issued 1 REC, which is tradable with utilities, for each 1MWh of energy produced (REC is named differently in different countries). Likewise, it is the common theme between the various P2P energy trade platforms whether in operation or under development to manage energy trade between peers and third parties by means of trading RECs, or equivalent tokens, efficiently and securely.

Some of such platforms utilize third party for transactions auditing, while the more advanced platforms are built on Blockchain technology to realize near-instant decentralized payment and auditing of transactions without the need for a third party.

About the authors:

Dr. I. A. Gowaid received the B.Sc. (First Class Hons.) and M.Sc. degrees in electrical engineering from Alexandria University, Egypt, in 2007 and 2011, respectively. From 2013 to 2017 he was with the Power Electronics, Drives, and Energy Conversion (PEDEC) Research Group, University of Strathclyde as a PhD candidate then as a postdoctoral research associate. He was a teaching assistant (currently on leave) at the Department of Electrical Engineering, Alexandria University as of 2008. He is currently with the Department of Electrical and Electronic Engineering, Glasgow Caledonian University as a lecturer of electrical power engineering. His current research interests include power electronics, solar and wind energy integration, high voltage DC transmission (HVDC), smart grids, and power system dynamics. Over 8 years of active research, Dr Gowaid has co-authored a number of highly-cited publications in top-ranked journals and conferences in the field of electrical power engineering.



Dr. Ahmed Aboushady received his B.Sc. (Hons) and MSc degrees in Electrical and Control Engineering from the Arab Academy for Science and Technology, Egypt in 2005 and 2008 respectively. Following this, he obtained his PhD degree in power electronics from the University of Strathclyde, Glasgow in 2013. He is currently a Lecturer in power electronics at Glasgow Caledonian University, UK and the MSc programme lead in Electrical Power Engineering. Dr. Aboushady has over 10 years of lecturing and research experience in power electronics and its applications. As principal investigator, he has been awarded a number of projects totalling over £0.5m from Scottish Power Energy Networks, Energy Technology Partnership and Oil and Gas Technology Center on new wireless charging technology applications and technology assessment of subsea DC power electronic systems for the offshore oil and gas sector. Dr. Aboushady had successful industrial collaborations in the past with Aker Solutions, Technip Umbilicals and Alstom Grid, and has published over 20 technical papers in refereed journals and conferences, a single-authored book, a book chapter contribution and a PCT patent. To date, he supervised 4 PhD students, a postdoctoral researcher and a number of master students. Dr. Aboushady is a senior member of IEEE, and his main research interests are in medium and high voltage DC transmission systems, integration of renewable energy systems and wireless power transfer applications.

The Challenges and Risks Facing ICT in the Management and Operation of the Smart Grid

Tarek M. Attia

National Telecom Regulatory Authority (NTRA), K28, Cairo-Alex. Desert Road, Smart Village, Giza, Egypt.

tattia@tra.gov.eg

Abstract - The Smart Grid integrates the traditional electrical power grid with information and communication technologies (ICT). Such integration empowers the electrical utilities providers and consumers and improves the efficiency and the availability of the power system while constantly monitoring, controlling and managing the demands of customers. Through the Smart Grid, the power system becomes smart by communicating, sensing, controlling and applying intelligence. It also keeps the environment free from pollution; minimizes the cost; and ensures effective operations against all types of hazards and danger. Smart Grid is a huge complex network composed of millions of devices and entities connected with each other through wireless communications techniques including Home Area Networks (HANs) and Wide Area Networks (WANs). Such a massive network comes with many security concerns and vulnerabilities. This paper highlights the complexity of the Smart Grid network and the challenges that exist in securing the smart power grid and the countermeasures and solutions applied for information and communication networks to secure Smart Power Grid. The paper concluded by overviewing the key functions and benefits of using the Smart Grid technology and how this affects human livelihood, economy and the environment.

Keywords - Smart Grid, Information and Communication Technologies (ICT), Challenges and Risks, Security and Privacy.

I. INTRODUCTION

The basic concept of Smart Grid is to add monitoring, analysis, control, and communication capabilities to the national electrical delivery system to maximize the throughput of the system while reducing the energy consumption. The Smart Grid will allow utilities to move electricity around the system as efficiently and economically as possible. It will also allow the home owner and business to use electricity as economically as possible.

Recent advancement in communication and

information technologies turned the way of operations in different fields such as healthcare, industries, transportation, environment, logistics, power grids, banking, etc.... and the Smart Grid can be considered one of the main applications of Internet of Things (IoT) Technology.

Smart Grid technologies have been used to distribute and upgrade electricity through two-way communications and pervasive computing capabilities for improving reliability, control, safety and efficiency. Smart Grid delivers electricity between consumers and suppliers and control digital appliances to save energy and increase efficiency, reliability and transparency. It provides protecting and automatic monitoring for interconnected elements. It covers generators via transmission network and distribution system for industries and home users with their thermostats and other intelligent appliances [1].

Smart Grids provide electricity demand from the centralized and distributed generation stations to the customers through transmission and distribution systems. The grid is operated, controlled and monitored using ICT. These technologies enable energy companies to seamlessly control the power demand, allow for an efficient and reliable power delivery at reduced cost and reduce transmission losses. These technologies recover fault automatically and reduce transmission lines. Smart Grid technologies are effective and beneficial for modern power systems in terms of technical solutions and economical point of view. They can integrate the renewable energy and distributed sources. The system is real time and two ways with theft detection capabilities. Various different technologies have been adopted by Smart Grid such as sensor networks, wireless mesh networks and intelligent and other interconnected technologies.

Basically, the Smart Grid concept is to provide grid observability, create controllability of assets, and enhance security and performance with cost-effective operations, maintenance and system planning. Through Smart Grid technology, the new grid is

expected to provide self-corrective, reconfiguration and restoration capabilities.

An intelligence Smart Grid system autonomously collects real-time data, analyzes them by using information about cyber security, computational intelligence, electricity generation, substations, distribution and consumer consumption, and provides secure, safe and reliable control. Data information from various terminals is electrically interconnected with a utility domain that is handled by the Supervisory Control and Data Acquisition (SCADA) system which has recently begun to spread in the world, especially in developed countries, as a practical model. Electrical information network protocol is a part of SCADA that helps in monitoring, controlling, configuration and troubleshooting the electric power networks. It can track disturbance in real time which means power grid should be responsive, awake and communicative with every node in the network [13].

Recently, the increasing demand for power transfers over long distance has emphasized the significance of stability in the power grid. Stability is referred to the ability of the grid to withstand disturbances through the nature of disturbance of interest. To address these challenges, power industries and government have been established to overcome and handle the issues with designing future grids. There are many challenges that hinder the efficiency of Smart Grid operation. Security remains one of the most important issues in Smart Grid systems given the danger and inconvenience residents and companies alike might encounter if the grid falls under attack. To understand the importance of exploring security and privacy issues in the Smart Grid which is one of the IoT applications, one must first take a look at the existing state of the IoT device deployments in the world. A study by Hewlett-Packard [2] on commercialized IoT deployments found that 80% of such devices violate privacy of personal information (e.g., name, date-of-birth, etc.), 80% failed to require passwords of sufficient complexity and length, 70% did not encrypt communications and 60% had security vulnerabilities in their user interfaces.

Three main security objectives must be incorporated in the Smart Grid system [3]: 1) availability of uninterrupted power supply according to user requirements, 2) confidentiality of user's data, and 3) integrity of communicated information.

The remainder of this paper is organized as follows. Section 2 provides a brief background about Smart Grid technologies. Section 3 discusses the key threats and challenges of Smart Grids. Section 4 explains the countermeasures and security solutions of Smart Grid. Section 5 provides a brief discussion of the key functions and benefits of the Smart Grid, and Section 6 summarizes the paper contributions.

II. SMART GRID TECHNOLOGIES

The National Institute of Standards and Technology (NIST) proposed a Smart Grid architecture composed of seven domains (bulk generation, transmission, distribution, customers, service providers, operations and markets) as shown in figure 1[4]. Each domain includes different Smart Grid actors. The Smart Grid infrastructure is divided into smart energy subsystem, information subsystem and communication subsystem. The Smart Grid can be viewed as having two main components; system component and network component.

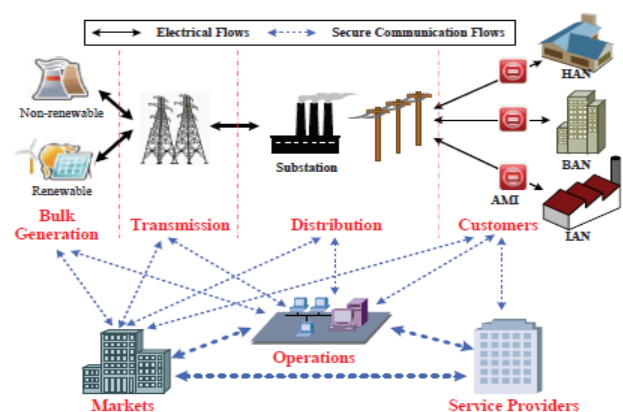


Fig .1 Domains of a smart grid [NIST]

1. System Components

The major system components in Smart Grid are Renewable Energy Resources, Distributed Energy Resources, Smart Meter, Electrical Household Appliances, Electric Utility Center for monitoring and controlling operation and Service Providers.

- Electrical Household Appliances are assumed to be able to communicate with smart meters via a HAN facilitating efficient power consumption management to all home devices.
- Renewable Energy Resources are solar, nuclear, coal and wind energy that supply home appliances with local generated electricity.

- Smart Meter is a stand-alone embedded system. Each smart meter contains a micro controller that has a memory, analogue/digital ports, timers, real-time clock and serial communication facilities. Smart meters register the power consumption periodically and transmit it to the utility server, connect or disconnect a customer power supply and send out alarms in case of abnormality. Some smart meters are equipped with relays that can be interfaced directly with smart home appliances to control them; for example, turn off the air conditioner during peak periods. Furthermore, the smart meter can be used in demand side management.
- Electric Utility Center interacts with smart meters to regulate power consumption. It also sends consumption related instructions to smart meters and collects sub-hourly power usage reports and emergency/error notifications using GSM/GPRS/3G/4G or WiMAX technology.
- Service Providers establish contracts with users to provide electricity for individual devices. Service providers interact with internal devices via messages relayed by the smart meter. To establish such interaction, service providers should register with the electric utility and obtain digital certificates for their identities and public keys. The certificates are then used to facilitate secure communications with users.

2. Network Component

In general, Smart Grid communication technologies are divided into 5 main areas: sensing and measurement, advanced components, decision support and improved interfaces, standards and interacted communications [1]. Smart Grid distributes the electricity between traditional and distributed generation resources to the residential, industrial and commercial consumers.

Through communication infrastructure, the smart monitoring and metering approaches provide real-time energy consumption. Via communication infrastructure, the Smart Grid intelligent devices, dedicated software and control centers interact with each other. The role of communication infrastructure is crucial for effective Smart Grid

operations. Smart Grid incorporates two types of communication: Wide Area Network (WAN) and Home Area Network (HAN). A HAN connects the in-house smart devices across the home with the smart meter. The HAN can communicate using ZigBee, Wi-Fi, wired or wireless Ethernet, or Bluetooth. On the other hand, a WAN is a bigger network coverage that connects the smart meters, service providers and electric utility. The WAN can communicate using WiMAX, GSM/GPRS/3G/4G and 5G (in the near future), or fiber optics and power line communication (PLC).

ZigBee, Ethernet, Wi-Fi, GSM, General packet radio services (GPRS), 3G, 4G and WiMAX are promising wireless and wired technology are currently used as integrated Smart Grid systems for communication management due to some distinctive advantages. For example, ZigBee WSNs are employed due to their low improved scalability, reliability and low cost [5]. Long Term Evolution (LTE), WiMAX and 4G are also among the new generation of wireless communication technologies with significant area of wider application in Smart Grid operational realizations. From the perspective of broadband communication system performance, LTE and 4G are more advantageous because of their bidirectional communications characteristic with wider network potential coverage suitable for widespread terminal access and remote control [6].

Technologies used for communication have a wide application field intensity according to the coverage range and data transmission rate. These technologies are shown in Table1. In order to find opportunities in real life applications of the designed model, a module must be determined for data transmission to be carried out smoothly in the Smart Grid.

The smart meter acts as a gateway between the in-house devices and the external parties to provide the needed information. The electric utility manages the power distribution within the Smart Grid, collects power usage from smart meters, and sends notifications to smart meters once required.

Table 1 Comparison between Different Communication Technologies [1, 3, 5, 6].

Technology	Frequency Band	Data Rate	Coverage Range	Limitations
GSM	900, 1800MHz(licensed)	Up to 14.4Kb/s	1–10km	Very low data rates
GPRS	900, 1800MHz(licensed)	Upto170Kb/s	1–10km	Low data rates
3G	1900, 2100MHz(licensed)	384Kb/s -2Mb/s Up to 168 Mb/s (HSPA+)	1–10km	Costly spectrum fees, Latency
4G	900,1900,2100, 2600MHz (licensed)	Up to 300Mb/s	Up to 5km	Costly spectrum fees
WIMAX	2.5GHz,3.5GHz,5.8GHz	Up to100Mb/s	10-50km(LOS) 1–5km(NLOS)	Not widespread
PLC	1–30 MHz	NB-PLC: 500 Kb/s BB-PLC: 200 Mb/s	NB-PLC: 150 km BB-PLC: 1.5 km	Noisy channel environment
WI-FI	Unlicensed frequency bands (2.4GHz and 5GHz)	Up to 150Mb/s	30–250m	High interference, Short range, High power consumption
ZigBee	868–915MHz, 2.4 GHz	250Kb/s	30–50m	Low data rates, Short range

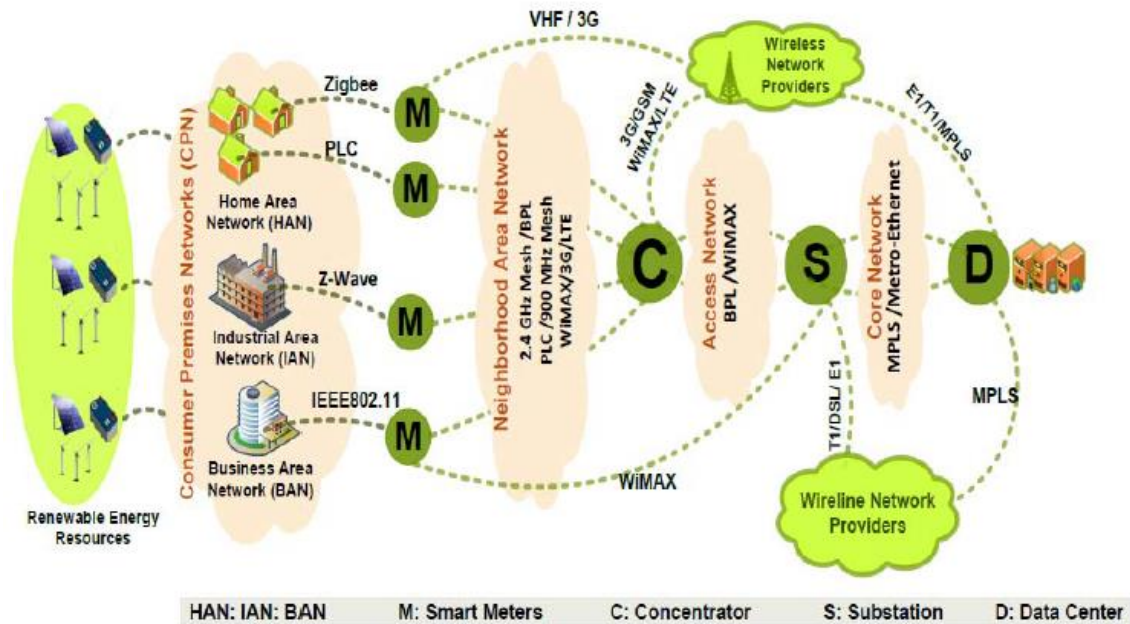


Fig .2 Basic network architecture [3]

The smart meter receives messages from devices within HAN and sends them to the appropriate service provider. Figure 2 illustrates the basic network architecture [3]. Note that while HANs are used in residential homes, Industrial Area Networks (IANs) and Business Area Networks (BANs) are used within industrial sites and business offices, respectively.

These technologies are designed to support Smart Grid applications in terms of controlling and monitoring operations as SCADA, Energy

Management Systems (EMS), Distribution Management Systems (DMS), Enterprise Resource Planning Systems (ERPS), distribution feeder automation, generation plant automation, physical security, etc.

III. KEY THREATS AND CHALLENGES

Smart Grid is a mixture of different legacy systems paired with new technologies and architectural approaches, based on different standards and regulations that all need to be integrated into a

communication network to support the challenges of the future electricity network. To support this objective, the cyber security architecture for Smart Grid communications is presented on the basis of cyber security and architecture requirements, dependency on legacy installations, and the regulations and industry standards. The Smart Grid can offer enormous economic benefits, but it faces many challenges, some of which are briefly described below.

1. Identity Management

A Smart Grid has several intelligent devices that are involved in managing both the electricity supply and network demand. These intelligent devices may act as attack entry points into the network. Moreover, the massiveness of the Smart Grid network makes network monitoring and management extremely difficult.

Access control is related to identity management, mutual authentication is needed to ensure that both suppliers and consumers can be sure of the other party's identity. Identity verification is about linking identities to real world properties, e.g. the physical location of a sensor, or the full name and postal address of an object.

2. Objects safety and security

The Smart Grid consists of a very large number of perception objects that spread over large geographic area, it is necessary to prevent the intruder's access to the objects that may cause physical damage to them or may change their operation. There are some limitations for the objects, for example [7]:

- Computational and energy constraint: Most of the time, Smart Grid devices are battery driven and devices that are using low-power CPUs have low clock rate. Therefore, computationally expensive cryptographic algorithms (that require fast computation) cannot be transferred directly to such low powered devices.
- Memory constraint: Smart Grid devices are built with limited RAM and Flash memory compared to the traditional digital system (e.g. PC, Laptop, etc.), and use Real Time Operating System or lightweight version of General-Purpose Operating System. They also run system software and proprietary services. Therefore, security schemes should be

memory efficient. However, traditional security algorithms are not designed specifically considering the memory efficiency, because the traditional digital system uses sizeable RAM and hard drive. Those securities schemes might not get enough space in memory after booting up the operating system and system software. Therefore, conventional security algorithms cannot be used directly for securing devices.

- Tamper Attacks: Smart Grid devices might be deployed in the remote regions and are left unattended. An attacker might tamper with the Smart Grid devices by device capture. Later, they can extract the cryptographic secrets, modify programs, or replace them with malicious nodes. Tamper resistant packaging is one way to defend against these attacks [2].

3. Data confidentiality

Smart meters autonomously collect massive amounts of data and transport them to the utility company and service providers. These data include private consumer information that might be used to deduce consumer's activities, devices being used and times when the home is vacant.

Data confidentiality refers to the prevention of data access by unauthorized persons or entities. Maintaining data availability involves ensuring that no person or entity could deny access to those authorized users and systems [14]. The sensor devices perform independent sensing or measurements and transfer data to the information processing unit over the transmission system. It is necessary that the sensor devices should have proper encryption mechanism to guarantee the data integrity at the information processing unit. The Smart Grid network determines who can see the data, thus, it is necessary to guard the data against external hackers.

4. Network security

The data from sensor devices is sent over wired or wireless transmission network. The transmission system should be able to handle data from a large number of sensor devices without causing any data loss due to network congestion, ensure proper security measures for the transmitted data and prevent them from external interference or monitoring [15]. There are some limitations for the security of the network, for example:

- Scalability: The number of Smart Grid devices is growing continuously and more devices are getting connected with the global information network. Current security schemes lack of the scalability property; therefore, such schemes are not suitable for Smart Grid devices.
- Diversity of devices: Diversity of the devices within the Smart Grid network ranges from the low-end RFID tags to full-fledged PCs. Therefore, it is hard to find a single security scheme that accommodates even the simplest of devices.
- Diversity of communication medium: Smart Grid devices connect to the local and public network via a wide range of wireless links. Therefore, it is difficult to find a comprehensive security protocol considering both the wireless and wired medium properties.
- Multi-Protocol Networking: Smart Grid devices might use a proprietary network protocol (e.g., non-IP protocol) for communication in proximal networks. At the same time, it might communicate with a Smart Grid service provider over the IP networking. These multi-protocol communication characteristics make traditional security schemes unsuitable for Smart Grid devices [2].
- Dynamic network topology: A Smart Grid device might join or leave a network at anytime from anywhere. The temporal and spatial device adding and exiting characteristic makes a network topology dynamic. Existing security model for the digital systems does not cope with these types of sudden network topological changes. Hence, such a model does not fit in with the smart device security.

5. Interoperability and Standardization

Many manufacturers provide devices using their own technologies and services that may not be accessible by others. The standardization of the Smart Grid network is very important to provide better interoperability for all objects and sensor devices and all components of Smart Grid. Using IP standards in Smart Grids offer a big advantage as they provide compatibility between the various components. However, devices using IP are inherently vulnerable to many IP-based network attacks such as IP spoofing, Tear Drop, Denial of Service (DoS), and others [7].

It can be envisaged that in a complex system such as Smart Grid, heterogeneous communication technologies are required to meet the diverse needs of the system. Therefore, the standardization of communications for Smart Grid means making interfaces, messages and work flows interoperable. Instead of focusing on or defining one particular technology, it is more important to achieve agreement on usage and interpretation of interfaces and messages that can seamlessly bridge different standards or technologies. In other words, one of the main aims of communication standardization for Smart Grids is ensuring interoperability between different system components rather than defining these components (meters, devices or protocols).

6. Deficiency of Policies and regulations

some countries already build smart cities with Smart Grids but still they are not clear to set the policies, regulations, guidelines and standards. The implementation of Smart Grids is another challenge because of its complicated design, planning and maintenance and operations. Only well organization with professional staff government organization can perform these tasks effectively. Inefficient and unorganized communication between teams might cause a lot of bad decisions leading to much vulnerability [1].

To educate the customers about Smart Grid operations and other services is another challenge. Cyber security technologies are not enough to achieve secure operations without policies, regulation and training.

7. Network Availability

Smart Grid services must be available at all times and Remote access to grid devices should be monitored and controlled. Since Smart Grid uses IP protocol and TCP/IP stack, it becomes subject to DoS attacks and to the vulnerabilities inherent in the TCP/IP stack. DoS attacks might attempt to delay, block, or corrupt information transmission in order to make Smart Grid resources unavailable.

8. Efficiency and Scalability

Ensuring system availability is a high priority in critical systems like the Smart Grid which requires that several key issues be addressed. First, the system

must be efficient in its use of computation and communication resources so that resources do not get dominated and all requests can be handled. Second, the system must have adequate redundancy built into it so that, if sub-systems fail or are compromised, then the entire system does not collapse. Third, the system should support auxiliary security functions that may be deployed in the Smart Grid communication system to detect and to respond to cyber-attacks [8]. Fourth, the system must have good error management built in to ensure proper handling of failures (e.g., those resulting from bad messages).

9. Impact of Interference due to Transmission Lines on Wireless Medium

One of the concerns in using wireless communication along power lines is the interference from high-voltage transmission lines. Electromagnetic noise generated around high-voltage power lines is an undesirable disturbance, which can affect wireless data transmission. This noise can be observed as an additive signal to the original one, and it can interrupt, obstruct, degrade, or limit the performance of communication systems [9].

10. Limitations based on software

These limitations include for example:

- **Dynamic security patch:** Installing a dynamic security patch on the Smart Grid devices and mitigating the potential vulnerabilities is not a straightforward task. Remote reprogramming might not be possible for the Smart Grid devices, as the operating system or protocol stack might not have the ability of receiving and integrating new code or library.
- **Embedded software constraint:** Operating systems, which are embedded within the Smart Grid devices, have thin network protocol stacks and might lack enough security modules. Therefore, the security module designed for the protocol stack should be thin, but robust and fault tolerant.

11. Jamming and Access Restriction

A jamming attack is used to prevent meters from connecting with the utility company through stuffing the wireless media with noise. This can be implemented in two methods: continuous noise signal emission

causing the channel to remain blocked; and noise signal emission only in response to the sensing of normal radio channel signals. Smart meters are affected in two corresponding ways: The channel can always be seen as engaged by carriers; and data packets are prevented from being received [10].

12. Frequency Spectrum scarcity

The Smart Grid devices require dedicated spectrum to transmit data over the wireless medium. Due to limited spectrum availability, an efficient dynamic cognitive spectrum allocation mechanism is required to allow millions of sensors to communicate over the wireless medium.

IV. COUNTERMEASURES AND SOLUTIONS

Security is a major challenge because the Smart Grid systems are controlled through the digital communications network, where important and private data are disseminated and stored. So, there is a need for a proper mechanism to ensure security and privacy in systems. The security and cyber securities are major challenges of recent Smart Grids systems.

Having overviewed the major challenges and vulnerabilities of Smart Grid, this section outlines some measures and solutions on cyber security for Smart Grid communications [3]:

1. Identity should be verified through strong authentication mechanisms

Organizations should implement an implicit deny policy such that access to the network is granted only through explicit access permissions. Moreover, each object/sensor needs to have a unique identity over the Internet. Thus, an efficient naming and identity management system is required that can dynamically assign and manage unique identity for such numerous objects.

2. Malware protection on both Embedded and General-purpose systems

Embedded systems are intended to only run software that is supplied by the manufacturer. The manufacturer is required to embed in its products a secure storage that contains keying material for software validation. Using a key, the system can validate any newly downloaded software prior to running. However,

general purpose systems are intended to support third party software. For this system, up-to-date and frequently updated antivirus software along with host-based intrusion prevention are required.

3. Network Intrusion Prevention System (IPS) and Network Intrusion Detection System (IDS)

technologies should augment the host-based defence to protect the system from outside and inside attacks. It is important to guarantee the real time performance and continuous operation features in a Smart Grid communication system.

4. Vulnerability assessments

They must be performed at least annually to make sure that elements that interface with the perimeter are secure. In some instances, user actions can open potential system vulnerabilities. As such, awareness programs should be put in place to educate the network users about security best practices for using network tools and applications.

5. Public Key Infrastructure (PKI)

Devices must use PKI to secure communication. However, there are some constraints regarding cryptography and key management. Current devices do not have enough processing power and storage to perform advanced encryption and authentication techniques, communications in a Smart Grid system will be over different channels that have different bandwidths, and connectivity, where all devices, certificate authorities, and servers must be connected at all times.

6. Special design and operation of Smart Grid

Security must be part of the Smart Grid design. Otherwise, security of devices becomes vendor specific; the fact that might produce many vulnerabilities because of incompatibility issues. Moreover, third-party companies can help for managing communication and data security issues of data transfer if network communications become a burden to the utilities.

7. Robust Authentication Techniques for Smart Grid includes

- Authentication protocol: A robust authentication

protocol is needed while communicating between Smart Grid parties. The protocol must operate in real-time abiding with some constraints such as minimum computational cost, minimum communication overhead, and robustness to attacks, especially DoS attacks.

- Devices must know the sources and destinations they communicate with: This is accomplished through mutual authentication techniques using Transport Layer Security (TLS) or Internet Protocol Security (IPsec). In addition, devices should support Virtual Private Network (VPN) architectures for secure communication.

8. Customer training

The government of any country must take the initiative for trainings and programs where customers will be taught about Smart Grids, its benefits and potentials. Print and electronic media are the main sources to educate customers and highlight the advantages and the benefits of using Smart Grid technologies.

9. Services resilient

With the very large numbers of sensors and actuators expected, it is inevitable that some fail, either through hardware faults, electrical noise or even mishandled upgrades. Services need to be designed to be resilient in the face of such failures. This needs to happen at multiple levels of abstraction. Resilience is also important for handling rapid changes in demand without overloading the platforms the services are running on. Resilience is also key to handling cyber-attacks. One approach to counter this is defense in depth with successive security zones for detecting intrusion and raising the alarm. Continuous monitoring can be combined with machine learning techniques for spotting unusual signs of behavior.

Cyber-attacks on Smart Grid devices are inevitable and the resilience of devices and networks must be carefully considered. Separation of valuable network assets may be the best way to protect them from attacks.

10. Privacy measures

Smart Grid should only collect the data needed from the huge amount of transferred data to achieve their goals and it is necessary to take proper privacy

measures and prevent unauthorized access. Some potential design principles are proposed to address privacy issues in the Smart Grid:

- An organization should ensure that information security and privacy policies and practices exist and are documented and followed. Audit functions should be present to monitor all data accesses and modifications.
- Organizations should ensure the data usage information is complete, accurate, and relevant for the purposes identified in the notice.
- Privacy policies should be made available to service recipients. These service recipients should be given the ability to challenge an organization's compliance with their state privacy regulations and organizational privacy policies as well as their actual privacy practices.
- Only personal information that is required to fulfil the stated purpose should be collected from individuals. Treatment of the information should conform to these privacy principles.
- Personal information should be used only for the purposes for which it was collected and should not be disclosed to any other parties except for those identified in the notice, or with the explicit consent of the service recipient.
- Personal information in all forms, should be protected from unauthorized modification, copying, access, use, loss, theft, or disclosure and notice should be announced before collecting and sharing personal information and energy use data.
- Information should only be used or disclosed for the purpose for which it was collected and should only be disclosed to those parties authorized to receive it. Personal information should be aggregated or anonymized wherever possible to limit the potential for computer matching of records.

V. THE KEY FUNCTIONS AND BENEFITS OF THE SMART GRID

The Smart Grid has to operate in a highly efficient manner, with higher liability and enhanced power quality. This key feature offers a lot of advantages and future perspectives in the power energy domain. One

of the main characteristics of Smart Grid is to keep a self-healing feature while relying on more renewable energy based generations systems such as solar and wind.

Customers will have better control and responsibility toward their power consumption. Due to its self-healing action, long outages will not occur. Smart Grids will be more efficient and economical than the existing power system because they will facilitate more renewable energy source integration. Figure 3 is an overview of Smart Grid key functions [11].

Monitoring and forecast of the supply-demand balance can be done in order to maintain the balance of supply and demand in energy production and consumption in the Smart Grid. Storing energy with photovoltaic cells and PV power units offers a wide range of opportunities in the network control in the provision of supply-demand balance in the micro-grid network [11]. The status of materials that are used in power generation and distribution of transmission is important for continuity of electrical energy. Also, energy can be used efficiently by coordinating production, transmission, distribution and storage.



Fig .3 Key functions of Smart Grid

Providing security of supply in the network raises the issue of energy efficiency. The customer also has a great responsibility alongside energy efficiency starting from subscriptions until delivery to the subscriber in an optimized way. Subscriber will contribute to this process by the selection of equipment and using it at convenient times. Keeping in mind the balance of the entire system constructed by the network structure will disclose itself. Consumers would support more longevity of the network and the effective protection minimizing technical losses by changing habits and drawing energy from the network overtime. Average energy consumption from the main supply and demand of energy taken under the energy efficient use of resources can be done with Smart Grid

management. In case of the production of renewable energy more efficiently, the use of energy storage is an alternative idea. Giving priority to renewable energy sources will reduce carbon emissions (CO₂). The balance of supply and demand in the network can be met by storing the energy while providing priority to renewable energy sources.

The grid will gain a dynamic structure by providing a controlled flow of power in distribution networks.

There are many benefits by using Smart Grid networks instead of traditional Grid, for examples:

- Reduce energy consumption costs by reducing energy consumption at peak time and to define the amount of energy that must be purchased based on real data and production plans.
- Reduce energy consumption by comparing energy consumption with production level: when a reduction in the production output is not matched by a corresponding reduction in energy usage, this must trigger energy managers to seek the waste source, and then take action to remove it [12].
- Improving the efficiency and the availability of the power system while constantly monitoring, controlling and managing the demands of customers.
- Improving maintenance management efficiency by identifying patterns in energy consumption and taking proactive maintenance considers when energy consumption goes consistently out of range.
- Improving the environmental effect and reputation of the factory by measuring and reducing the CO₂ footprint of production processes.
- Continuous improvement of energy efficiency at the production level by decentralizing decision-making.
- Monitoring power quality in factories by monitoring energy in real-time and informing the energy provider about power fluctuations occurrences.
- Increasing energy-aware process design in both the short and the long term by integrating energy data into process design to reduce energy waste.

- Improving the economics of self-generated power by the efficient use of renewable energy; for example, using weather forecasting to build production schedules relying on energy that is expected to be generated and requiring energy for production [12].

VI. FUTURE RESEARCH DIRECTION

Future research efforts involving ICT for Smart Grid management and control functions should focus on a number of critical issues. Since Smart Grid concept use distinct and advanced communication architectures, therefore issues regarding operational readiness, communication security, system responsiveness, management of increased number of communication nodes in the network, the routing protocols in communication networks for Smart Grid between in-home smart appliances, smart meter and the operator's control center, ease of system deployment and extended network coverage should be given preference. Future research on sensor design and measurement in intelligent network architecture should focus more on a high degree of sensitivity, security and reliability that ensures higher information integrity at the consumer terminal, as well as reliable feedback for central control of the tool and management system. The achieving of these functions highly depend on innovations of new and advanced microelectronic technologies and control methods, improved energy conversion and storage systems and applications of integrated power electronics devices. Further studies are needed to enhance the security level of the grid including integrity and confidentiality of the transmitted data, and enhancing universal policies and regulations for secure communication technology. Finally, there is also need to improve the time required to perform speedy fault diagnosis which can basically be achieved by improvement in interfaces and decision support technologies.

VII. CONCLUSIONS

Traditional power systems are moving towards digitally enabled Smart Grids which will enhance communications, improve efficiency, increase reliability and reduce the costs of electricity services. Smart Grid technology is a beneficial technology for power system stability, customer's satisfaction, load distribution and all types of grid operations. The emergence of Smart Grid technologies will give favorable environment for future, better power

supplies services. Clearly, securing the Smart Grid communication infrastructure will require the use of standards-based state-of-the-art security protocols.

The massiveness of the Smart Grid and the increased communication capabilities make it more prone to cyber-attacks. Since the Smart Grid is considered a critical infrastructure, vulnerabilities and challenges should be identified and sufficient measures and solutions must be implemented to reduce the risks to an acceptable secure level. This paper was used to identify interesting multiple issues of importance to Smart Grid cyber security. This paper also surveyed the challenges, threats and vulnerabilities in Smart Grid networks, and the solutions needed as countermeasures to these challenges. An observed trend was that many of the attacks were almost identical in their function, but they are simply applied to the grid in different ways.

REFERENCES

- [1] R.M. Larik, M.W. Mustafa and S.H. Qazi. "Smart Grid Technologies in power systems: An overview." *Research Journal of Applied Sciences, Engineering and Technology*, vol. 11(6), pp 633-638, 2015.
- [2] M. Hossain, M. Fotouhi, and R. Hasan. "Towards an analysis of security issues, challenges, and open problems in the Internet of things." 2015 IEEE World Congress on Services, New York, 2015, pp. 21-28.
- [3] F. Aloul, A.R. Al-Ali, R. Al-Dalky, M. Al-Mardini and W. El-Hajj. "Smart Grid Security: Threats, vulnerabilities and solutions." *International Journal of Smart Grid and Clean Energy*, vol. 1, No. 1, September 2012.
- [4] J. Liu, Y. Xiao, S. Li and W. Liang. "Cyber security and privacy issues in Smart Grids." *IEEE Communications Surveys & Tutorials*, vol. 14, No. 4, Fourth Quarter, pp.981-997, 2012.
- [5] S. Elyengui, R. Bouhouchi and T. Ezzedine. "The enhancement of communication technologies and networks for Smart Grid applications." *International Journal of Emerging Trends & Technology in Computer Science (IJETTCS)*, vol.2, Issue 6, pp. 107-115, November-Dec.2013.
- [6] Y.S. Mohammed, N. Bashir, A. Mohammed and A.K. Benjamin. "Information and communication technology for control and management in power systems Smart Grid." *International Journal of Engineering and Innovative Technology (IJEIT)*, vol. 2, Issue 5, pp. 214-220, November 2012.
- [7] R. Khan, S.U. Khan, R. Zaheer and S. Khan. "Future Internet: The Internet of things architecture, possible applications and key challenges." in 10th International Conference on Frontiers of Information Technology Proceedings, 2012, pp. 257-260.
- [8] Ye Yan, Yi Qian, H. Sharif and D. Tipper. "A survey on cyber security for Smart Grid communications." *IEEE Communications Surveys & Tutorials*, vol. 14, No. 4, pp.998-1010, Fourth Quarter 2012.
- [9] A. Pawar and S. Rahane. "Opportunities and challenges of wireless communication technologies for Smart Grid applications." *International Journal of Computer Networking, Wireless and Mobile Communications (IJCNWMC)*, vol. 3, issue 1, pp. 289-296, Mar 2013.
- [10] C. Lopez, A. Sargolzaei¹, H. Santana¹ and C. Huerta. "Smart Grid cyber security: An overview of threats and countermeasures." *Journal of Energy and Power Engineering*, vol. 9, pp. 632-647, 2015.
- [11] R. Bayindir, I. Colak and K. Demirtas. "Smart Grid technologies and applications." *Renewable and Sustainable Energy Reviews* (66), pp.499-516, December 2016.
- [12] F. Shrouf and G. Miragliotta. "Energy management based on IoT: Practices and framework for adoption in production management." *Journal of Cleaner Production*, pp.1-12 (2015).
- [13] P. Thapa, S. K. Acharya, H.I. Chang, S. Park, H.S. Jung, O.I. Whan, G.C. Park and J. Lee. "A high-speed intelligence Smart Grid system by using MIMO channel capacity." *International Journal of Advances in Computer Networks and Its Security(IJCNS)*, vol. 7, issue 1, pp. 113-117, April 2017.

- [14] I. Ali, S. Sabir and Z. Ullah. "Internet of things security, device authentication and access control: A review." International Journal of Computer Science and Information Security (IJCSIS), vol. 14, No. 8, pp.456-466, August 2016.
- [15] T. Attia. "Challenges and opportunities in the future applications of IoT technology." 2nd MENA Regional ITS Conference, Egypt on 18 – 21 February 2019, pp.1-15.

Modelling and Energy Analysis of Solar Charging Facility for Electric Vehicles in Chile

Scarlett Allende

Los Zarzales 1533, Santiago 9270842. Chile.

ssallend@uc.cl

Abstract - This paper presents simulation and energy evaluation of a photovoltaic charging centre intended to supply the demand of 244,000 electric vehicles in Chile. According to the obtained results, the transportation system was feasible from the solar radiation, energy consumption, geographic zone, type of PV farm and other sources. Notably, the studied region has a solar potential to supply 10% of the total domestic cars existing in Santiago, providing a total energy of 253.723 GWh/yr. Furthermore, based on the study factors, the design of the system consists of approximately 428,590 PV modules and an average power generation of 31.89 W/hour for one single module. Finally, the configuration of a solar charging facility allows applying a new method of energy supply to electric cars that improves the environmental conditions of the city and encourages sustainable development in the transport sector.

Keywords - Electric cars, Photovoltaic, Energy demand, Solar radiation, Design system, Power generation.

I. INTRODUCTION

One of the crucial issues addressed in the big cities is the number of petrol vehicles and the pollution produced. There are several reasons to continue improving the transportation system through electric cars that are considered as an alternative solution friendly to the environment. At the same time, electric cars allow the analysis of the potential of the system based on the solar resource of a geographic zone.

Overall, Chile has severe issues of air pollution, of which 30% is the result of the transport emissions [1]. Therefore, the implementation of innovative technologies of transport and the clean energy

generation are crucial to help supply the demand of energy and decrease the levels of pollution in the city.

On the other hand, Chile has enormous potentials in solar energy and consequently in the development of electric vehicles. Currently, the Chilean government has used its solar potential to create sustainable initiatives, such as the "Electrolinera" project that involves the construction of 14 charging PV centres designated to solar cars [2].

II. METHODOLOGY

1. Estimating Energy Demand

There are eight procedures to obtain the energy data, as shown in Figure 1. Firstly, the route is selected on the smartphone by a route application (such as "Runtastic"), then it applied driving in a diesel car in the streets in Santiago. After that, the application generated graphs of speed (km/hr) and altitude (m).

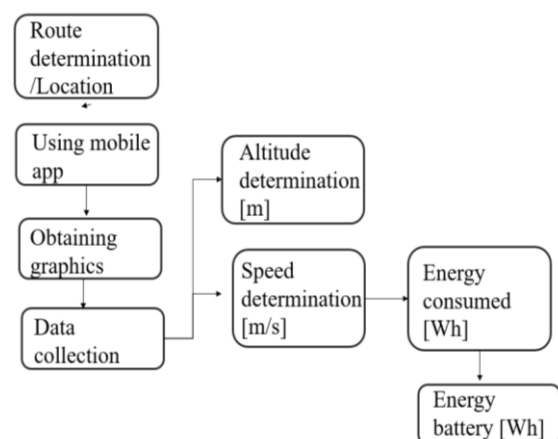


Fig .1 Flow diagram to obtain the energy demanded by the battery.

$$E = \left[(\mu * m * g * \cos\theta) + (m * g * \sin\theta) + \left(\frac{1}{4} C_d * A * \rho * (V_f^2 + V_i^2) \right) \right] * \Delta d + \frac{1}{2} * m * (V_f^2 - V_i^2)$$

Eq .1: Energy consumption by the car [3].

Where, m : mass of the car; A : Is the frontal area of the car (2.754 m^2 [3]); C_d : is the drag coefficient of the car (with 0.272 [3]); μ : is the traction efficiency of the surface (0.8 factor [4]); ρ : is the density of air kg/m^3 (1.225 kg/m^3 [5]); θ : is the slope angle; Δd : Is the difference of distance; g : is a gravitational constant equal 9.81 m/s^2 ; V_f : Final velocity; V_i : Initial velocity. At the same time, the angle of the slope is calculated with the altitude data by Equation 2.

$$\theta = \frac{(\tan^{-1} * (\Delta \text{distance})) [m]}{\Delta \text{Altitude} [m]}$$

Eq .2: Angle of the slope in radians

At the same time, throughout the route, the energy consumption was variate by the regenerative and traction braking. Therefore, it is necessary to calculate the energy consumption considering ranges of efficient of the vehicle. The function represented in Equation 3. Where, η_{bc} : is battery charging efficiency; η_d : Discharging efficiency; η_c : Charging efficiency, E_t : Energy of traction and E_{reg} : Energy of regeneration. In this case, it was considered a discharging factor of 0.85 [3], charging factor of 0.7 [3] and a battery charging efficiency of 95% [3]

$$\text{Energy} = \left(\frac{1}{\eta_{bc}}\right) \left[\left(\frac{1}{\eta_d}\right) E_t - \eta_c * E_{reg} \right]$$

Eq .3: Total trip energy calculation [3]

Once obtained the value of energy battery (considering regenerative and traction efficiencies), it is necessary continuing with the calculation of average distance and energy consumed, as shown in Figure 2. At the same way, determining the number of electric vehicles is essential, which represents 10% of the domestic cars existing in the city.

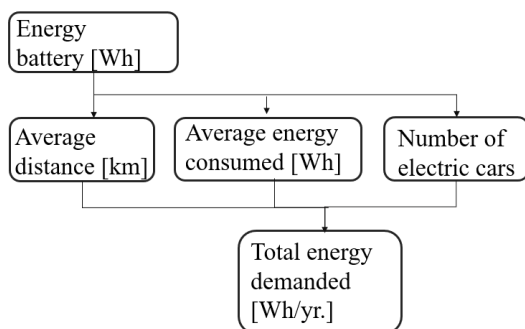


Fig .2 Flow diagram to calculate the total energy demanded.

Following, Equation 4 is used for the calculation of total

demand energy, which involves the following factors. D : is the average driving distance (2.964 km); n : represents the number of electric vehicles (150) and E_{avg} : is the average energy consumption of an electric car (961.06 Wh). In this case, the number of electric cars considered is represented by the project "Electrolinera" in Chile [2]

$$E_{total} = D * n * E_{avg}$$

Eq .4: Total energy demand [6]

2. Calculation of Temperature and Irradiation

The calculation method performed for the output power of the PV module detailed in Figure 3. Those involve obtaining the data of temperature and solar source. Furthermore, it is necessary to consider PV modelling aspects, such as cell temperature and its efficiency.

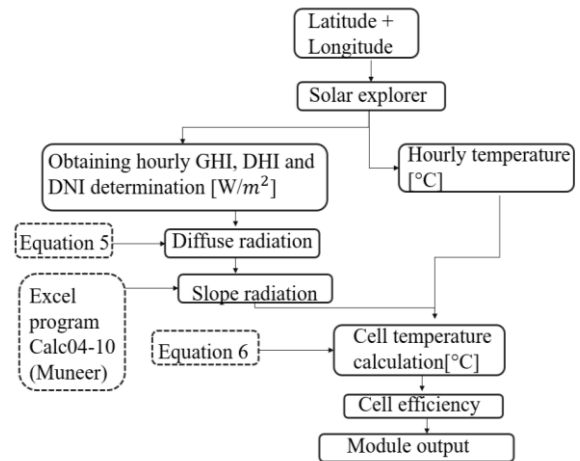


Fig .3 Flow diagram to calculate the module power output.

The first step is to obtain the latitude and longitude by "google map", in this case, it was -33.52° and -70.76° , respectively. Then, the coordinates data entered in the solar explorer [7] provide the data of temperature and irradiation by day and hour, in a direct way. With the data of global and direct Irradiation the diffuse radiation can be calculated by the following formula.

$$GHI = DifHI + DHI$$

Eq .5: Calculation of diffuse radiation [8]

Specifically, GHI is the global horizontal irradiation W/m^2 , and DHI is the direct horizontal irradiation W/m^2 . With the difference of both Irradiations, the diffuse radiation W/m^2 is obtained. Once collecting

all the radiations, it was possible to calculate the slope irradiation by Excel program Calc 04-08 (Muneer). After this step, the cell temperature is measured, considering the ambient temperature hourly, slope irradiation and other factors shown in Equation 6.

$$T_c = T_a + \left(\frac{G_{slope}}{G_{noct}} \right) (T_{c, noct} - T_{a, noct}) \left(1 - \left(\frac{\eta_{stc}}{\tau \alpha} \right) \right)$$

Eq .6: Calculation of cell temperature [9]

Where, G_{slope} : Global slope irradiation; G_{noct} : 800 W/m²; $T_{c, noct}$: Cell temperature at NOCT; $T_{a, noct}$: Air temperatures NOCT; η_{stc} : Cell efficiency at SCT; $\tau \alpha$: Absorptivity of the module and T_a : Ambient temperature.

By Equation 7 is possible to calculate the PV cell efficiency under determinants of temperature fluctuations, efficiency at standard test conditions (η_{stc}), Cell temperature (T_c), Cell temperature under standard test conditions ($T_{c, stc}$) and temperature coefficient value (ap) [9].

$$\eta_{cell} = \eta_{stc} [1 + ap(T_c - T_{c, stc})]$$

Eq .7: Calculation of cell efficiency [9]

The last estimation is the electrical output power represented in Formula 8, whose factors are η_{mod} : Electrical efficiency under standard test conditions, A :

Surface area of PV panel, G_{tilt} : consists on slope irradiation, and finally, T_c : Cell temperature calculated in the step before.

$$P = \eta_{mod} * A * G_{tilt} [1 - 0.0045 * T_c - 298.15]$$

Eq .8: Calculation of output performance [10]

III. RESULTS

1. Unit Demand

Firstly, the data collected in the route chosen were a total of 5.7 km of distance and at a time of 13 minutes and 20 seconds. According to the results, the speed was relative during the driven route with ranges between 0.5 and 16 m/s, and the average velocity was of 7.62 m/s.

Figure 4 indicates the different road gradients which variation is between the values 0 to over 400m. Seeing the definition of altitude in the graph, it can be assumed that the route was ascending most of the time. With this database, it was possible to calculate the angle of the gradient (rad) to obtain energy consumption finally. Besides, the illustration shows the performance of energy consumed on the route. Some of these values are negative due to the retrieved energy which was generated by regenerative braking, and the positive values represent the energy consumed, which involves traction efficiency. The average energy consumption of the trip was of 961.06 Wh.

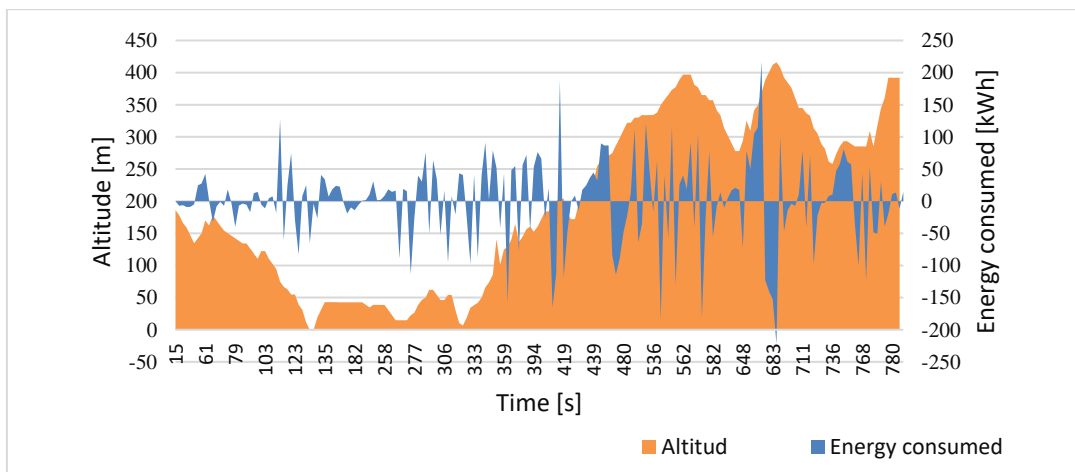


Fig .4 Altitude of the route and energy consumed by the battery.

2. National Demand

The total energy consumed per year was 253.7 GWh, considering supplying 244,000 electric cars

per year. The details of the performance result can be seen in Table 1.

Table 1. Summary of Total Energy Demanded

Average distance km	Average E consumed Wh	E total demand GWh	E total demanded GWh/yr.
2.964	961.06	0.6951	253.7

3. Calculation of Temperature and Solar Source

The hourly temperature data were obtained by solar explorer [7] considering coordinate of latitude -33.5 and longitude -70.7. The days measured by solar explorer were between the dates 1st Jan 2016 and 26th Dec 2016. However, only the data that belong to the 12th day of each month will be considered.

Figure 5 shows the elevated difference between the maximum and minimum temperature during the

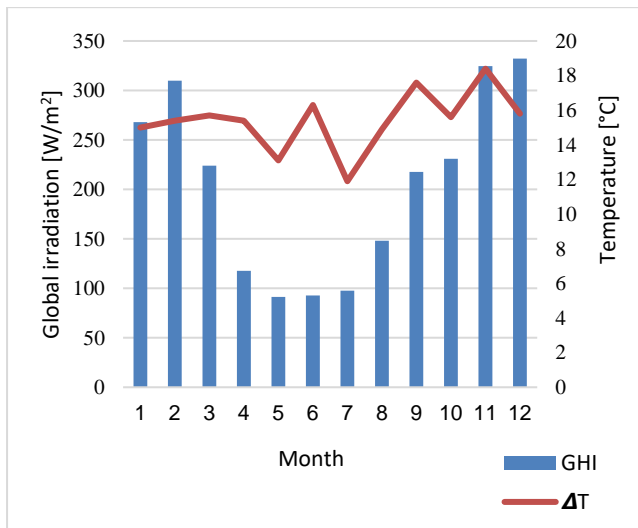


Fig. 5 Average hourly corresponding to the global horizontal irradiation (W/m^2) and the difference between the maximum and minimum ambient temperature (W/m^2) for the entire year.

year, which was around 18 °C in the spring season. A similar procedure was applied to get the hourly irradiances, obtained by the solar explorer [7]. As described in Figure 5 the best radiation performance is in the summer season (between November and February) with over 300 W/m^2 of global irradiation. In the rest of the months, steady rises and drops exist.

On the other hand, the hourly global irradiation result showed that the maximum average of radiation is between 12 and 16 hours with over 500 W/m^2 . Figure 6 describes the minimum performance, which is during morning and evenings when the global radiation declines dramatically. Additionally, it represents the output power of a single PV module, whose peak is at 17 hours with more than 80W.

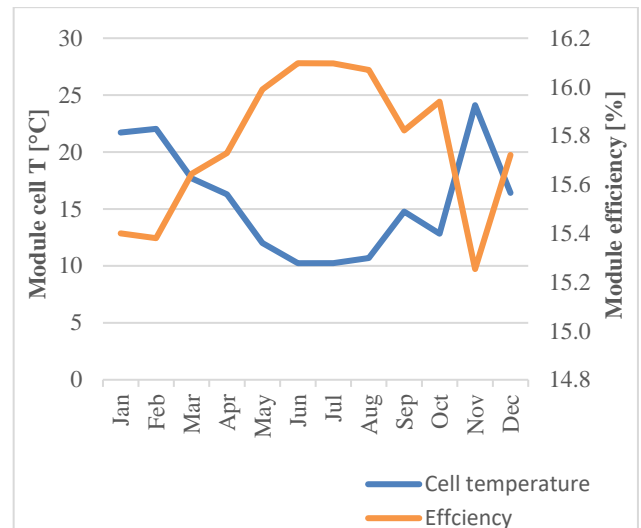


Fig. 7 Comparison between cell temperature and panel efficiency.

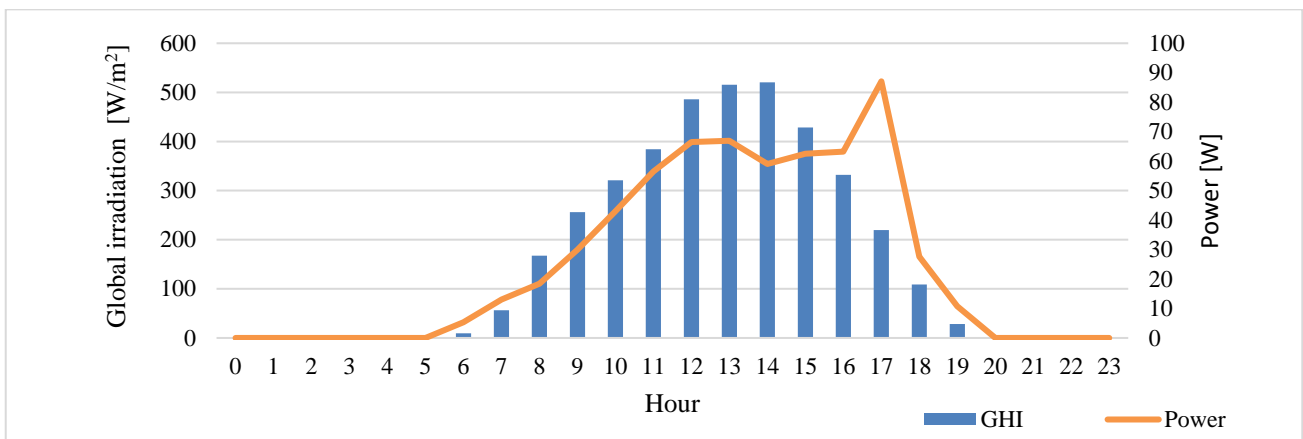


Fig. 6 Annual average of GHI per hour (W/m^2) and average of PV output power (W).

4. Calculation of Cell Temperature

After obtaining the temperature and irradiation per hour, the cell temperature was calculated considering the values G_{slope} calculated previously; G_{noct} : 800 W/m² [9]; T_c of 47 °C [11]; T_a , $T_{a, noct}$ of 25 °C [11]; n_{stc} of 15.2% [11]; $T\alpha$ of 0.8 [11] and T_a , calculated earlier. Figure 8 describes the relationship between ambient temperature and cell temperature per hour.

The following result was the calculation of cell efficiency of the PV panel, and it was reached by Formula 7, which involved factors of n_{stc} of 15.20%; T_c , stc of 25 °C; α_p of 0.40 %/°C and T_c calculated in the step before. Figure 7 demonstrates the relationship between cell temperature and panel efficiency.

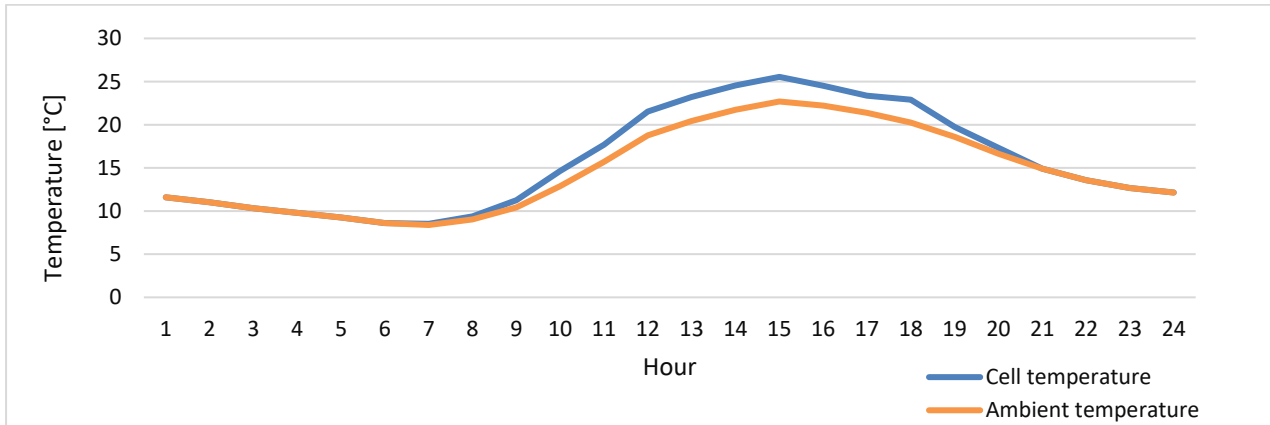


Fig .8 Comparison between cell temperature and ambient temperature.

5. Determination of the PV System

A. PV modules quantity

Firstly, it was necessary to estimate the energy produced by one PV module, through Formula 9. The Equation involves factors of PV surface area (2.6 m² [11]), the efficiency of the system (15.20% [11]) and tilted global irradiance (7.92 kWh/m²).

$$E_{module} = A_m * \eta_{sys} * I_{tilt}$$

Eq .9 : Energy of PV module [3].

Where A_m represents the useful PV area; η_{sys} is the efficiency of the system and I_{tilt} is the tilted global irradiance calculated previously. The next step is to calculate the number of PV modules necessary to supply the total consumption, which is obtained by Equation 10.

$$X_{min} = \frac{E_{total\ consumption}}{E_{module}}$$

Eq .10: Number of PV modules.

As a result, Table 2 shows a summary of the number of PV modules required. The function involves the total energy consumption per year whose value was

253,723,041.351 kWh/year and the energy produced by one PV module was 591.99 kWh/yr., obtaining 428,590.713 modules overall.

Table 2. Summary of the Number of PV Modules.

E module/year kWh	Total consumption kWh/year	Number PV Module
591.99	253,723,041.351	428,590.713

B. Calculation of array size

Besides, it was necessary to measure the maximum open circuit voltage of the module as shown in Equation 11. The factors are the V_{oc} that is open circuit voltage; $T_{dcu, mod}$ that represents the temperature voltage coefficient (0.4 [11]) and ΔT_{low} (-13.1 °C) which is the difference between the ambient temperature (7.5 °C) and T_c, stc (25 °C [11]). As a result, the maximum voltage in the open circuit is 55.45V.

$$V_{dc\ max\ mod} = V_{oc} * \left(1 + \left(T_{dcu\ mod} * \frac{\Delta T_{low}}{100} \% \right) \right)$$

Eq .11: Maximum voltage in open circuit [12].

At the same way, the minimum voltage in an open circuit can be calculated by Formula 12. Where, V_{mpp} is the maximum power of the PV module (49.25V); $T_{dc\ mod}$ is temperature voltage coefficient (0.4) and ΔT_{max} (3.5°C) represents the difference between the $T_{max, mod}$ and T_{set} . The minimum voltage open circuit is 49.94V.

$$V_{dc\ min\ mod} = V_{mpp} * \left(1 + \left(T_{dc\ mod} * \frac{\Delta T_{max}}{100} \% \right) \right)$$

Eq .12: Voltage minimum in open circuit [12].

Analogously, the maximum current of PV module was calculated by Equation 13, which involves the short-circuit current (I_{sc} of 7.92A [11]); current temperature ($T_{dc, mod}$ of 0.05 [11]) and the difference between the maximum module temperature and STC temperature, represented by ΔT_{max} (3.5°C). The I_{max} open obtained was of 7.93A.

$$I_{dc\ max\ str} = I_{sc} * \left(1 + \left(T_{dc\ mod} * \frac{\Delta T_{max}}{100} \% \right) \right)$$

Eq .13: Maximum current of PV module. [12].

Then the minimum number of strings was calculated through Equation 14, whose factors are: maximum power generated (P_{dcgen}); the maximum power of the module ($P_{max, mod}$) and the number of strings per module ($n_{mod\ str}$). The calculation considered a P_{max} of 54400W; $P_{max\ mod}$ of 13.9W and n_{mod} of 18 modules, obtaining a minimum number of strings of 217.

$$n_{min\ str} = \frac{P_{dcgen}}{P_{max\ mod} * n_{mod\ str}}$$

Eq .14: Minimum number of strings [12].

Finally, the total number of inverters was obtained by Equation 15, which includes the number of PV modules (n_{mod} of 3905.2) and the total number of strings (n_{array} of 428,591). In this case, the total of inverters was 110.

$$n_{inv} = \frac{n_{mod}}{n_{array}}$$

Eq .15: Total number of inverters [12].

C. Designing the PV facilities

The PV charging zone proposed in Santiago was located mainly in the western region of the city. The solar facilities placed around 2km of distance from the

route done. The place has plenty of areas available and no risk of obstruction of radiation. The availability of solar PV installation is 1,008,000m².

Around 60% of the mentioned area belongs to the PV facilities (576998.7437m² of a useful area), and another 20% of the surface is left unoccupied to allow the maintenance between PV panels, which is 201,600m². Furthermore, the PV modules installed will have a 45° inclination and orientated towards the north. According to the previous calculation, each charging station will have 18 rows and 57 columns. Also, the arrangement of 217 strings connected in parallel with 18 modules connected in series is considered. At the same time, one inverter manages 57 PV panels of one total of 428,591 PV modules.

IV. CONCLUSION

According to the transport and environmental plans of the Chilean government, the pollution problem is expected to be resolved. One alternative is by the promotion of solar charging facilities of electric cars, providing electricity for 10% of the national car fleet in Santiago. Specifically, the study demonstrated the following findings.

- The energy consumption has a direct relationship with the type route (altitude) and the speed. That is because in some parts of the road the cars needed acceleration and in other deceleration, causing more demand for energy consumption in the point of high altitude than others. At the same time, this produced an effect of regenerative braking and traction efficiency, which means negative and positive values of energy consumption.
- Overall, the solar analysis demonstrated that temperature and irradiation have a direct relationship. The maximum level of radiations is the summer season with maximum average values of global radiation of 340 W/m². Showing enough potential to supply the PV system.
- On the other hand, the results showed that throughout the day the solar module increases its temperature considerably, around 13% more than ambient temperature, between hours 15 and 16.
- At the same time, the cell efficiency was decreased by approximately 4% when the cell module got the maximum value of temperature. This period was

between October and November. However, global competence represents an excellent performance for the system.

- The best power performance of the PV module was between hours 18 and 19 (over 80W), increasing the output power by 27%.
- To supply the energy required is necessary to count for the excellent PV facilities. In this case, the installation of 428,590.713 photovoltaic modules and the integration of 20% of the area in the solar facilities, whose objective is maintenance of work and reduction the possibilities of obstruction in solar radiation are a must.

REFERENCES

- [1] G. Aymeric and S. François. "Case study for Chile: The electric vehicle penetration in Chile," in *Electric Vehicles: Prospects and Challenges*, 2017, pp. 245–285.
- [2] J. M. Vilches. "Emol," 2017. [Online]. Available: <http://www.emol.com/noticias/Tecnologia/2017/07/13/866601/El-panorama-de-los-autos-electricos-en-Chile-Cuantos-son-y-donde-se-cargan.html>. [Accessed 1st Oct 2018].
- [3] T. Muneer, R. Milligan, I. Smith, A. Doyle, M. Pozuelo and M. Knez. «Energetic, environmental and economic performance of electric,» *Transportation Research Part D: Transport and Environment*, Vol.35, pp 40-61, 2015.
- [4] CausaDirecta. (2013) "Investigación y reconstrucción de accidentes de tráfico." [Online]. Available: <https://causadirecta.com/especial/calculo-de-velocidades/tablas/tabla-de-factores-de-rozamiento-del-pavimento-para-neumaticos-de-goma>. [Accessed 8th Oct 2018].
- [5] WindPower. (2003) "Danish wind industry asociacion" [Online]. Available: <http://xn--drmstrre-64ad.dk/wp-content/wind/miller/windpower%20web/es/tour/wres/enerwind.htm>. [Accessed 8th Oct 2018].
- [6] D. Goos. "Feasibility study of a solar charging facility for electric vehicles in Munich." Master thesis, School of Engineering & the Built Environment Edinburgh Napier University, Edinburgh, 2015.
- [7] Facultad de ciencias físicas y matemáticas, Universidad de Chile, "Explorador solar," 2018. [Online]. Available: <http://ernc.dgf.uchile.cl:48080/exploracion>. [Accessed 11 Oct 2017].
- [8] R. Escobar, J. M. Cardemil, C. Cortés and A. Pino, "Atlas solar de Chile," Pontificia universidad católica de Chile, Santiago, 2013.
- [9] M. Jeffrey, I. Kelly, T. Muneer and I. Smith, "Evaluation of solar modelling techniques through experiment on a 627 kWp photovoltaic," School of Engineering and Built Environment, Edinburgh Napier University, Edinburgh, 2015.
- [10] D. a. Beckmann, *Solar engineering of thermal process*, Madison: University of Wisconsin, 1991.
- [11] Advanced Solar Photonics. "ASP-400GSM - Smart moduletm series - high efficiency frameless monocrystalline solar modules". (2012). [Online]. Available: <https://www.enfsolar.com/Product/pdf/Crystalline/50bd9203a2fc0.pdf>. [Accessed 1st Oct 2018].
- [12] S. Allende. "Energy Analysis of a Solid Oxide Fuel Cell (Sofc) Operated by PV System in the Residential Sector, in Highland." Master thesis, School of Engineering & the Built Environment, Edinburgh Napier University, Munich: GRIN Verlag, 2018.
- [13] S. Henriquez, "Red de electrolineras ya cubre en forma continua desde Coquimbo a Biobío".(2019). [Online]. Available: <http://www.economiaynegocios.cl/noticias/noticias.asp?id=550309>. [Accessed 1st Mar 2019].
- [14] Comisión Nacional de Energía. (2015), "Informe costos de inversión por tecnología de generación". [Online]. Available: <https://www.cne.cl/wp-content/uploads/2015/11/Informe-Costos-de-Inversi%C3%B3n-Tec-de-Generaci%C3%B3n-Ago-2015.pdf>. [Accessed 1st Oct 2018].
- [15] Comité Nacional, Gobierno de Chile (2017). "Estudio Benchmarking de plantas solares

- fotovoltaicas en Chile." [Online]. Available: http://www.comitesolar.cl/wp-content/uploads/2017/04/Informe-Benchmarking-Plantas-Solares-Fotovoltaicas_actualizaci%C3%B3n.pdf. [Accessed 16th Oct 2018].
- [16] Asociación Chilena de energías renovables. (2017) "Energía solar: prometedor futuro para Chile" [Online]. Available: <http://www.acera.cl/energia-solar-prometedor-futuro-para-chile/>. [Accessed 1st Oct 2018].
- [17] M.Gutierrez. (2017). "Economía y negocios." [Online]. Available: <http://www.economiaynegocios.cl/noticias/noticias.asp?id=341770>. [Accessed 8th Oct 2018].
- [18] J. V. F. Serra. «Electric vehicles: Technology, Policy and Commercial Development,» 1st ed. London: Routledge, 2012..
- [19] M. Mruzek, IgorGajdáč, L. Kučera and D.Barta. «Analysis of Parameters Influencing Electric Vehicle Range,» *Procedia Engineering*, vol. 134, pp.165-174, 2016.
- [20] E.S. Rubin and C.I. Davidson. *Introduction to Engineering and the Environment*, 1st ed. Boston: McGraw-Hill, 2001.
- [21] T. Muneer, C. Gueymard and H. Kambezidis. *Solar Radiation and Daylight Models*, 2nd ed. Amsterdam: Elsevier, 2004.

Voltage Clamping Circuits for Large Voltage Step-Down Coupled Inductor Converters

Richard Pollock

University of Strathclyde 16 Richmond St, Glasgow G1 1XQ, UK.

richard.pollock@strath.ac.uk

Abstract - Water desalination processes require power converters with large voltage step-down ratios and high efficiencies. Coupled inductor (tapped-inductor) circuits can achieve this where the whole inductor carries current during one switch state but only part of the inductor carries current during the second switch state. The switch state change results in excessive switch voltages due coupling leakage. To protect the switching device, a novel voltage clamp is presented which improves the overall efficiency of the switching circuit and recovers otherwise wasted energy. It requires no closed-loop control. For higher power levels, an asymmetric half-bridge coupled-inductor buck converter circuit, which offers switch protection without a snubber, is presented. The circuit is shown to offer reduced switching losses despite having two switching components in the high-voltage forward conduction path.

Keywords - asymmetrical half-bridge coupled-inductor buck converter, buck converter, coupled-inductor buck converter, reversible buck converter, tapped-inductor buck converter.

I. INTRODUCTION

Various methods, such as reverse osmosis, and multi-stage flash distillation, are used for water desalination. This research focuses on capacitive deionization (CDI) water desalination. The method requires a voltage less than 1.5V [1]: the Nernst voltage of water. For a saline solution of 2000 parts per million, CDI uses 66% less energy than reverse osmosis, which is the next best alternative method [2]. CDI requires the charging and discharging of a capacitor-like cell. This research investigates circuits that can achieve bidirectional current flow and a low-voltage output.

This low-voltage would typically be derived from a conventional domestic or industrial rectified AC supply. The coupled-inductor buck converter has been proposed as a circuit that can achieve the large step-down ratios desired: typically, in the range of 600:1. Circuits with large step-down ratios require protection on the main switch due to the leakage energy

associated with the coupled inductor. Two such variants of the coupled-inductor buck converter with switch protection are presented. In this research, the merits of a half-bridge circuit with two switches rated for full current, and a single-ended circuit requiring only one switch rated for the full primary current, but requiring a voltage clamp circuit to protect the primary switching device against a potential over-voltage while allowing the voltage to rise highly enough to enable efficient transfer of the stored energy to the secondary winding, are compared.

The paper is organized as follows. Section 3 documents derivation of the voltage transfer ratio of the coupled inductor circuit and shows why it is suitable for large voltage step-down ratios such as required in desalination. The new asymmetric half-bridge coupled-inductor buck converter is introduced in Section 4. Section 5 describes the single-ended magnetically-coupled converter, and introduces a voltage clamp with energy recovery to manage the leakage energy. Test results at a range of clamp voltages are presented. Section 6 compares the test results for the new asymmetric half-bridge with those for the voltage-clamped single-ended converter. Finally, the results are discussed in relation to the desalination process.

II. COUPLED-INDUCTOR BUCK CONVERTER

Power converters for water desalination processes can require step-down ratios in the order of 600:1. This arises where the input voltage is derived from a rectified three-phase supply at typically 600V, and a voltage of less than 1.5V is required to electrolyze a solution of impure water.

The coupled-inductor converter, Fig. 1, is a version of the buck converter which has a split or tapped inductor. In one circuit switching state, the whole inductor conducts the current. In the second circuit switching state, only part of the inductor conducts.

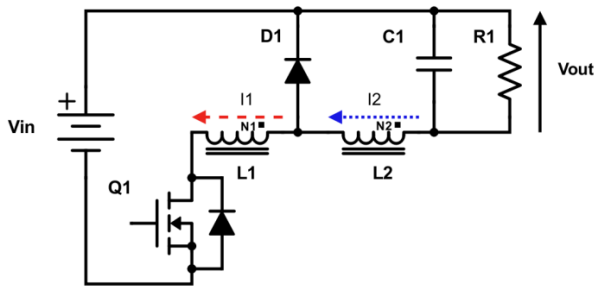


Fig .1 (a) Coupled-inductor buck converter [3].

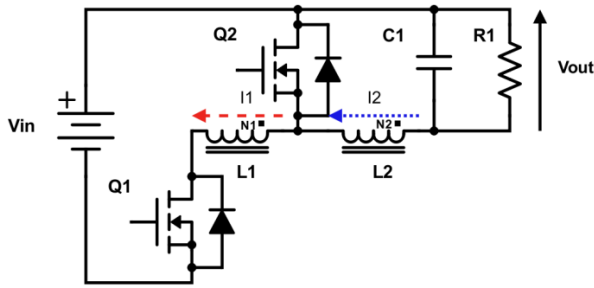


Fig .1 (b) Reversible coupled-inductor buck converter with synchronous rectification [3].

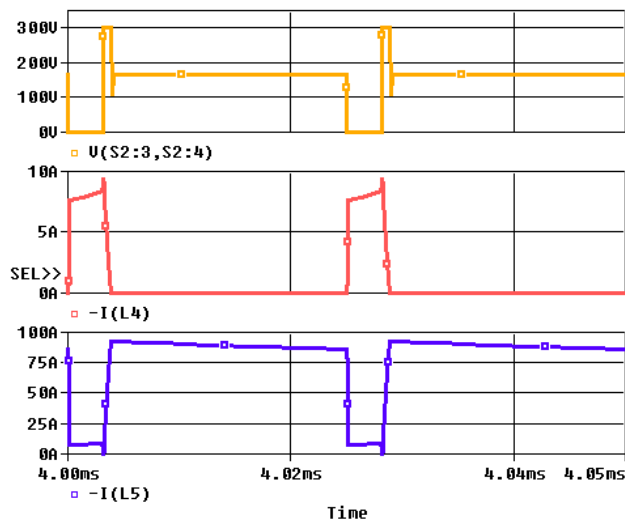


Fig .1 (c) Coupled-inductor buck converter simulation.

The input voltage V_{in} is converted to a significantly lower output voltage V_{out} . When the main single switch Q1 is turned on, current flows through the load R1 and the series-connected coupled inductor L1 with N_1 primary turns and N_2 secondary turns. During this time the flux in the core of the coupled-inductor increases as does the energy stored. Unlike the flyback converter [4], the coupled-inductor circuit's energy is provided to the load R1 during the on-time of Q1. The energy stored is the combined energy storage of the coupled inductors L1 and L2. When switch Q1 is turned off, all the stored energy becomes associated with the inductor L2 with turns N_2 . The current in L2 and

therefore the load current (via diode D1) decrease. The stored energy decreases whilst energy is delivered to the load.

L1 and L2 will never be 100% coupled and energy associated with the leakage inductance between these windings must be managed correctly when Q1 turns off. In single-switch converters such as those shown in Fig.1 the energy associated with the leakage inductance causes the voltage across the primary side switching device Q1 to increase when it is turned off.

In the coupled inductor, the voltage across L1 has to reverse and exceed the referred voltage of the secondary before energy can start to transfer to the secondary winding. In the single-ended converter the voltage across the primary switching device increases to a level in excess of the DC supply voltage. Due to the leakage inductance the voltage across Q1 has to rise further to absorb the additional energy stored in the leakage inductance which is not transferred to the secondary.

currents I_1 in L1 and I_2 in L2 are shown in the second and third plots of the simulations in Fig.1(c), where the inductors have 97.5% coupling. The voltage across the main switch Q1 rises to 300V.

III. VOLTAGE TRANSFER EQUATIONS OF COUPLED-INDUCTOR BUCK CONVERTER

The coupled-inductor buck circuit in Fig. 1 can be analyzed similarly to the standard buck converter circuit.

When the main switch Q1 conducts with duty ratio, δ :

$$V_{in} - V_{out} = \frac{L_{total}}{\delta T_s} (I_{1max} - I_{1min}) \quad (1)$$

When the main switch Q1 turns off:

$$V_{out} = \frac{L_2}{(1-\delta)T_s} (I_{2max} - I_{2min}) \quad (2)$$

The secondary inductance with N_2 turns can be expressed as a fraction of the total inductance ($L_{total}=L_1+L_2$):

$$L_2 = \left(\frac{N_2}{N_1+N_2}\right)^2 L_{total} \quad (3)$$

The MMF in the inductor must be continuous in either side of the switching boundary. Therefore:

$$(N_1 + N_2)I_{1max} = N_2I_{2max} \quad (4)$$

Using (3) and (4) the output voltage can be expressed as:

$$V_{out} = \frac{\left(\frac{N_2}{N_1+N_2}\right)^2 L_{total}}{(1-\delta)T_s} \times \frac{N_1+N_2}{N_2} (I_{1max} - I_{1min})$$

$$= \frac{N_2 L_{total}}{(1-\delta)T_s} (I_{1max} - I_{1min}) \quad (5)$$

Combining (1) and (5), and eliminating currents and period T_s :

$$\frac{V_{out}}{V_{in}} = \frac{\delta N_2}{N_2 + (1-\delta)N_1} \quad (6)$$

The voltage transfer function of the coupled-inductor buck converter therefore has the benefit of the inductor turns ratio in addition to the duty ratio δ of the main switch Q1 to achieve large step-down voltage ratios (c.f. similar to AC autotransformer action).

IV. ASYMMETRIC HALF-BRIDGE COUPLED-INDUCTOR CONVERTER

The converter shown in Fig. 2 is the asymmetric half-bridge version of the circuit shown in Fig.1(b). Two switches; Q1 and Q2, are used to apply the input voltage to the coupled inductor and output circuit. When Q1 and Q2 turn off, the current transfers into clamping diodes D1 and D2. This effectively changes the potential difference across the coupled inductor from V_{in} to $-V_{in}$ which creates an effective voltage swing of $2V_{in}$. Thus, the current transfer time is quicker than for the conventional coupled-inductor buck converter in Fig. 1(b). The current in primary winding L1 is forced to zero and the secondary current can flow in the synchronous rectifier Q3. Both switches Q1 and Q2 are protected from the effects of leakage inductance by their associated diodes, D1 and D2, which clamp them to V_{in} for Q1 and GND for Q2.

A coupled-inductor circuit driven by an asymmetric half-bridge uses the supply protect the main switching devices from over-voltage. Although the clamping circuit uses two switches and two diodes, the devices are all rated close to the input supply voltage. The additional switch is added just as in the two switch flyback converter [5], [6].

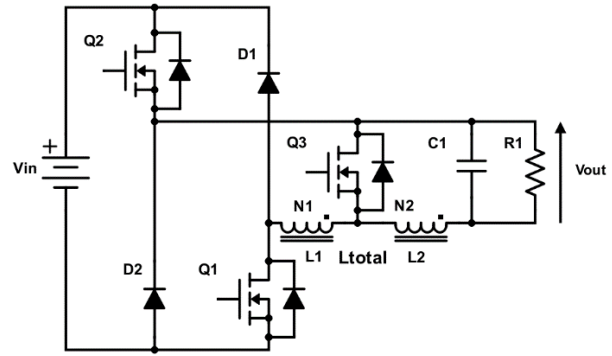


Fig .2 Asymmetric half-bridge coupled-inductor circuit.

In full-bridge or asymmetric half-bridge converters, the leakage energy is recirculated to the DC supply of the primary winding and the voltage across the switching devices is clamped to the DC supply voltage. However, two switching devices are required and there are therefore two device voltage drops in series in the primary current path.

1. Simulation of the Asymmetric Half-bridge

Fig. 3. shows simulation results for the asymmetric half-bridge coupled-inductor circuit in Fig. 2, where $V_{in}=200V$, $\delta=16\%$, $N1:N2=10:1$, $R1=4m\Omega$ and $C1=6.8mF$.

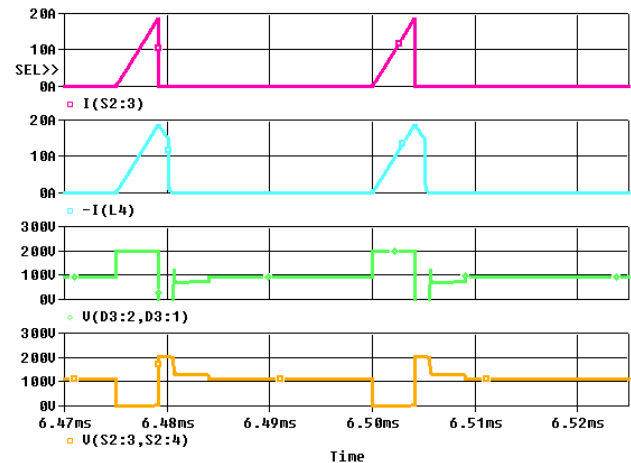


Fig .3 Simulated switching waveforms of the asymmetrical half bridge coupled-inductor buck converter.

V. SINGLE-ENDED CONVERTER WITH VOLTAGE CLAMP CIRCUIT

A second voltage clamp circuit, Fig. 4, is proposed to protect the main switch Q1 in Fig. 1 and provide a path to manage the energy associated with the leakage flux between L1 and L2. When the main switch Q1 is turned off, the current in the primary and secondary windings of the coupled inductor flows in diode D1, charging capacitor C2. At the same time, the

synchronous MOSFET Q3 turns on providing a lower voltage freewheel path for the current in L2. The circuit in Fig. 4 is similar to that in a previously proposed design [7], but in Fig. 4 C2 is referenced to the supply voltage which almost halves the required capacitor voltage rating. The voltage across C2 must be high enough to force the primary current to zero. At the end of the switching transition the current I_{2max} in L2 is given by (4). The time, t_{tr} , taken for the transfer of energy from the primary N_1 turns to the secondary N_2 turns is given by:

$$t_{tr} = \frac{L_{leakage} I_{1max}}{V_{C2} - \frac{N_1}{N_2} V_{out}} \quad (7)$$

In order for the energy to transfer from the primary L1 to the secondary L2, the voltage across C2 must be greater than the referred secondary voltage. A higher voltage across C2 leads to a shorter transfer time and reduces losses in the conductors of inductors L1 and L2. A higher voltage leads to higher switching losses in the main switch. There may therefore be an optimum value for the voltage across capacitor C2 which minimizes the losses on the primary side. This will be investigated in Section 6.

Voltage VC2 across C2 is controlled by the energy recovery switch Q2 in Fig. 4. Q2 provides a path to transfer capacitor energy to the input supply via inductor L3. An advantage of the voltage clamp is that it only activates at the controlled voltage level ($V_{in} + V_{C2}$) to protect the switching devices, and at that level, recycles excess energy back to supply V_{in} .

An advantage of using a clamp is that current only flows into the clamp when its threshold voltage is exceeded. This contrasts with an RC snubber [8], [9] which draws current under all operating conditions, and therefore reduces circuit efficiency. Additionally, a key benefit of the voltage clamp circuit is that the voltage across switch Q1 will not rise above the designed clamp voltage regardless of the load, thus ensuring the device is always safe from over-voltage. The voltage clamp is set at a voltage which is appropriate for the switch rating.

The voltage clamp circuit maintains a constant clamp voltage regardless of load, provided the energy recovery circuit is in continuous conduction. However, the clamp voltage will drop at lower loads when the energy recovery circuit enters discontinuous conduction.

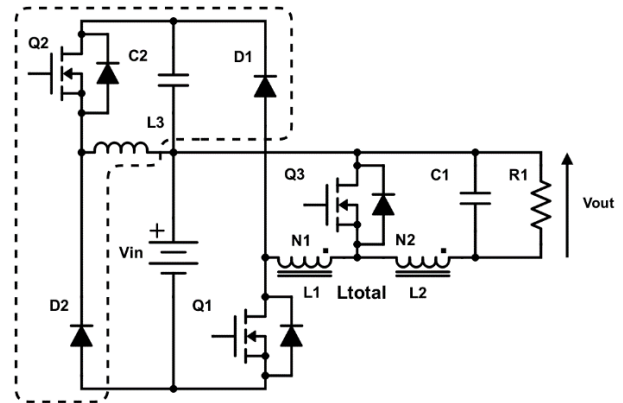


Fig. 4 Voltage clamp circuit for single-ended coupled-inductor circuit. Dotted line shows the added buck converter with capacitor C2 referenced to V_{in} .

1. Simulation of the Asymmetric Half-bridge

Fig. 5 shows typical simulation results for the coupled-inductor circuit with voltage clamp, shown in Fig. 4, where $V_{in}=200V$, $\delta_{Q1}=16\%$, $\delta_{Q2}=13\%$, $N_1:N_2=10:1$, $R_1=4m\Omega$, $C_1=6.8mF$, $C_2=470\mu F$ and $L_3=163\mu H$.

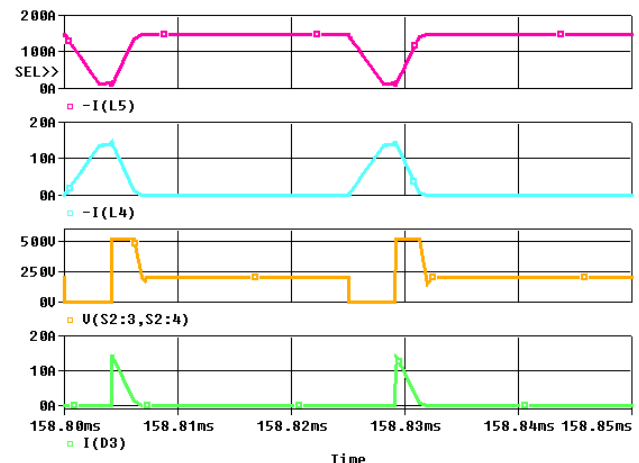


Fig. 5 Simulated waveforms for coupled-inductor buck converter with a clamp voltage of 385V.

VI. EXPERIMENTAL RESULTS

The main objective of the experimental study is to demonstrate that the practical circuits can achieve a high voltage step down in a single stage. At the present stage of development, the experimental setup allows for a step-down ratio of 100:1. Initial tests targeting an output voltage of 1.5V, requiring a duty cycle of 10%, were conducted successfully. Waveforms for these tests are not presented here, but power loss data was gathered. In addition to high-voltage step-down, high-power throughput is also desirable. The circuit was then configured to operate at a maximum power throughput given the limitations of the experimental prototype. Under these operating

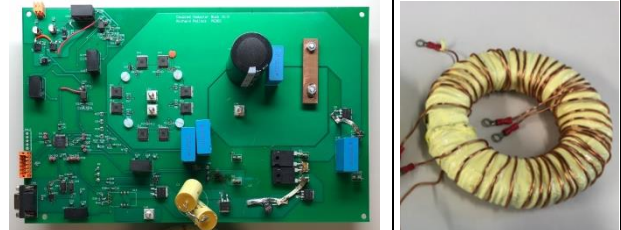
conditions, where the duty cycle is 16%, output voltage is 2.6V and power throughput is 300W. Experimental results are presented for these operating conditions. Power loss data was also gathered.

Both circuits shown in Fig. 2 and Fig. 4 were experimentally assessed to evaluate switching losses and conduction losses with the same input voltage, duty cycle, and coupled inductor turns ratio. The input voltage was 150V and the coupled inductor turns ratio was 10:1.

The switches were controlled via a board-mounted microcontroller to ensure minimal noise on the gates of the devices. The same PCB output stage consisting of C1, R1, Q3 and the coupled inductor L1 and L2 were used for both circuits to ensure a valid comparison between both circuits. The experimental components are detailed in Table 1.

Table 1. Component for Experimental Hardware, used for Both the Asymmetric Half-bridge and Single-ended Converter.

Name	Component	Model	Values	Rating
Q3	MOS Power Transistor	IPB100N		30V
Q1,2	Power MOSFET	IGW15N120H3		1700V
D1,2	TO-247 Diode	VS-40EPS12-M3		1200V
L1	Iron Powder Inductor	T520-52 core (10:1 turns ratio)	60.8mΩ 497μH	
L2	Iron Powder Inductor	Shared core with L1	2.6mΩ 4.7μH	



The experimental design and coupled inductor construction are also shown in Table 1. The PCB shown on the left was used for both the buck clamp snubber and later the asymmetric half bridge to ensure a fair comparison. The coupled inductor construction consisted of the primary being wound on the toroidal core with 120 turns and then two secondaries in parallel each of 12 turns wound on top of the primary turns. An additional layer of insulation was added to ensure isolation. The main design consideration of the coupled inductor is to minimise leakage inductance and maximize coupling.

As such the inductor terminations are kept as short as possible and the secondary turns are spread out to encompass as much of the core as possible.

1. Simulation of the Asymmetric Half-bridge

The asymmetric half-bridge with an input voltage of 150V gives a change of 300V (or $2V_{in}$) across the coupled inductor during the switching transition of the main switch Q1. To enable a comparison, the single-ended converter also requires 300V across the coupled inductor and so is controlled to have a clamp voltage of 300V, i.e. $V_{C2}=150V$. The conduction losses in the diodes are ignored as they only conduct for a very short period. The switching losses in the diodes are zero due to the fact the diode current falls to zero before the switch turns back on and a voltage is applied across the diode.

Fig. 6 presents results from the practical circuit configured and controlled to give an output voltage of 2.6V. From Fig. 6, it can be seen that as Q1 turns off its voltage rises from zero to 150 V whilst the diode voltage simultaneously falls from 150 V to zero and begins conducting. The voltage across the coupled inductor is the difference between the voltages across diode D2 and switch Q1. This demonstrates the 300V potential that is created across the coupled inductor in the transition period. The switch current (top trace) shows that when the switch Q1 is on all of the primary current flows through Q1. It can be assumed that Q2 conducts the same current. When switch Q1 turns off, the primary current does not fall to zero instantaneously but finds a current path through D1 and falls to zero over time. The experimental results shown are seen to follow closely those simulated in Fig. 3.

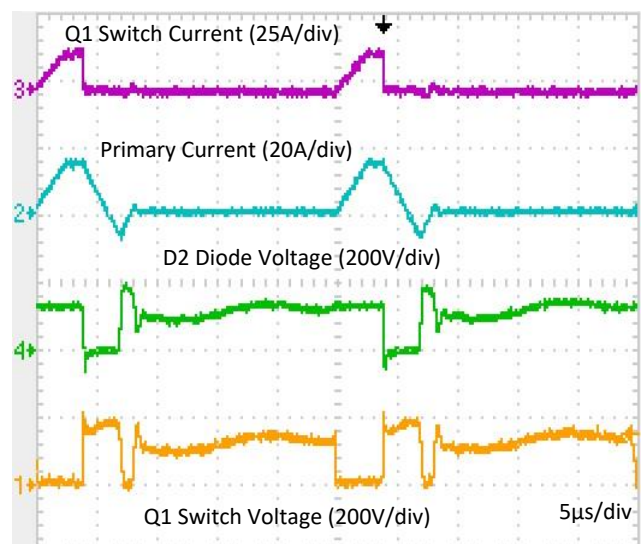


Fig. 6 Switching waveforms of the asymmetrical half-bridge coupled-inductor buck converter

Fig. 7 shows the detailed view of the turn-off waveform of Q1. This can be used to calculate the switching losses of switches Q1 and Q2. The switching losses are the product of the voltage across the switch multiplied by the current through it.

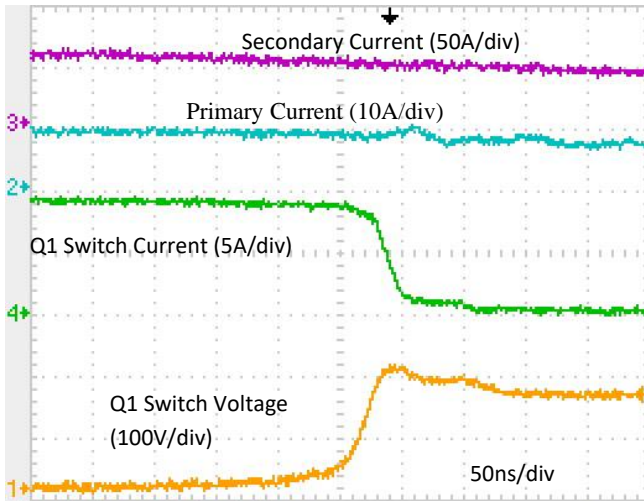


Fig. 7 Detailed switching waveforms of the asymmetrical half bridge coupled-inductor buck converter.

Table 2 presents loss information for the asymmetric half-bridge coupled-inductor buck converter operated with output voltages of 1.5V ($\delta=10\%$) and 2.6V ($\delta=16$). The results show that efficiency increases with power. This is due to the switching losses increasing by a smaller proportion than the increase in power. The secondary conduction loss increases approximately linearly with power and the primary loss increases fourfold.

Table 2. Asymmetrical Half-bridge Power Loss and Efficiency at 120W and 300W Output.

	120W (1.5V)	300W (2.6V)
Switching Loss	10.73W	11.87W
Primary Loss	0.43W	1.64W
Secondary Loss	12.17W	21.30W
One Switch Conduction Loss	3.32W	3.32W
Total Losses	29.98W	41.46W
Percentage Efficiency	74.05%	84.39%

2. Single-Ended Converter

In comparison with a passive snubber, such as RC snubber, the voltage clamp proposed in Section 5 and illustrated in Fig. 4 offers switch protection and improved efficiency in a single-ended coupled-inductor

converter. The voltage clamp can be controlled using the duty cycle of switch Q2 to determine the voltage of the clamp depending on the switch rating and application. The clamp circuit was tested at different voltages to assess its effect on performance and efficiency of the coupled-inductor buck converter. Readings were taken for clamp voltage varying between 250V and 385V.

A. Waveforms

Fig. 8(a) shows the waveforms for the coupled-inductor buck converter at a clamp voltage of 250 V, and Fig. 8(b) shows the same plots but for a clamp voltage of 385 V. By increasing the clamp voltage from 250V to 385V, achieved by varying the duty cycle of the clamp switch Q2, the rise time of the current in the secondary decreases 5.6 μ s to 2 μ s. Thus the circuit has the design value of output current flowing in the output R1 for a larger percentage of the switching cycle. In each case the voltage across Q1 is clamped to the chosen clamp voltage and the switch is protected from over-voltage. During this period current flows into the clamp circuit. The experimental plots in Fig. 8(b) also confirm the simulation results in Fig. 4.

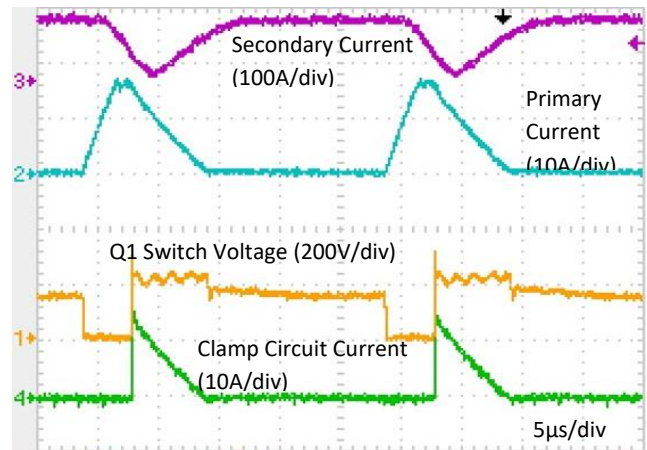


Fig. 8 (a) Circuit waveforms at clamp voltage of 250V.

Figs. 9(a) and 9(b) show detailed versions of Figs. 8(a) and 8(b) focused on the on-to-off transition of the main switch Q1. These were used to calculate switching losses.

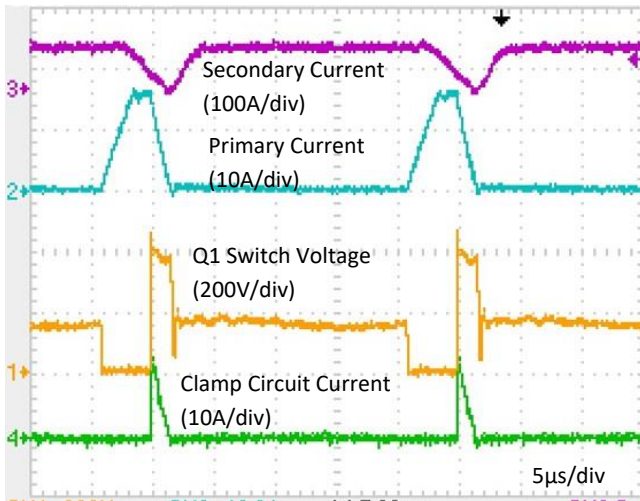


Fig .8 (b) Circuit waveforms at clamp voltage of 385V.

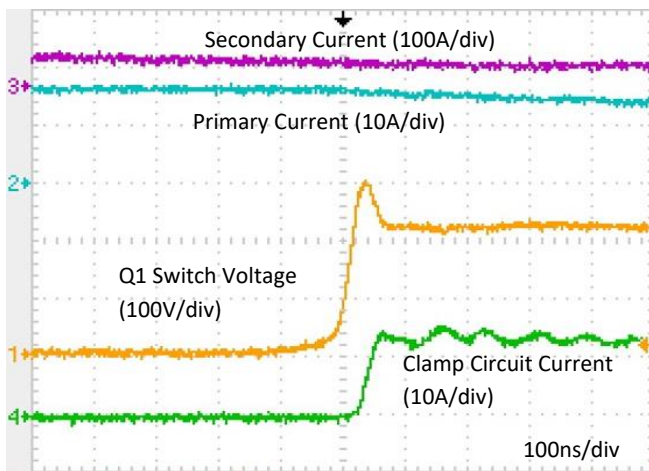


Fig .9 (a) Detailed view of circuit waveforms at clamp voltage of 250V

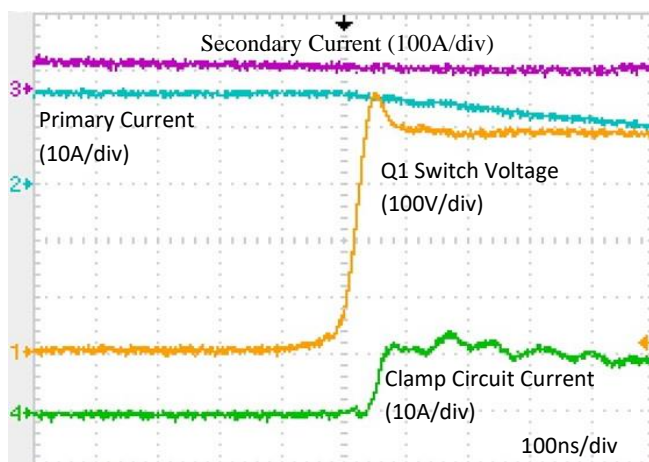


Fig .9 (b) Detailed view of circuit waveforms at clamp Voltage of 385V.

B. Data analysis

The clamp on the single-ended converter protects the switch from over-voltage, as shown in Figs. 8(a) and (b) where the voltage across the switch is controlled to a predefined value. Data was also collected to investigate the effect of clamp voltage variation on the efficiency of the circuit. Figs. 10(a) and (b) show the clamp current and voltage, respectively, which are used to calculate the instantaneous switching power loss shown in Fig. 10(c).

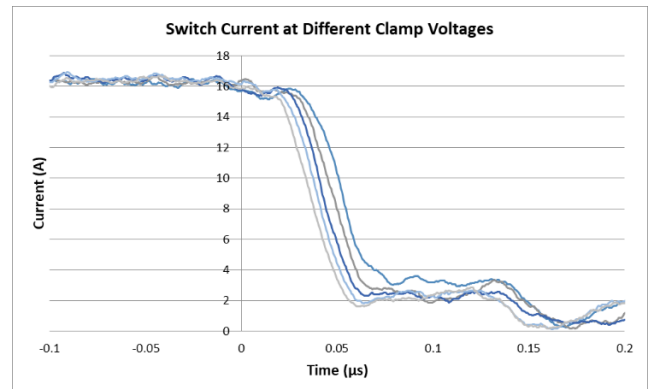


Fig .10 (a) Q1 turn off transition currents at different clamp voltages.

In Fig. 10(a), the highest clamp voltage of 385V creates the current that is slowest to fall whereas the lowest clamp voltage produces the quickest fall. In Fig. 10(b), the largest clamp voltage is 385V which produces the highest voltage across the switch and a clamp voltage of 210V produces the smallest voltage.

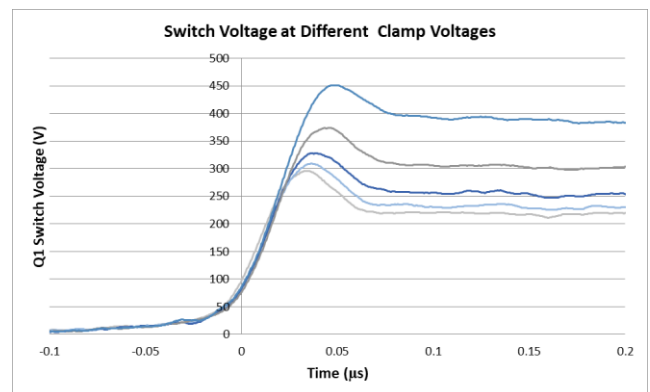


Fig .10 (b) Voltage across main switch Q1 at the turn off transition.

The results presented in Fig. 10(c) are calculated from the product of the switch voltage and current at a given time instant, for a given clamp voltage. The switching losses increase as clamp voltage is increased. This is due to the increase in current decay time as clamp

voltage is increased. The area under each plot gives the total switching loss for one transition.

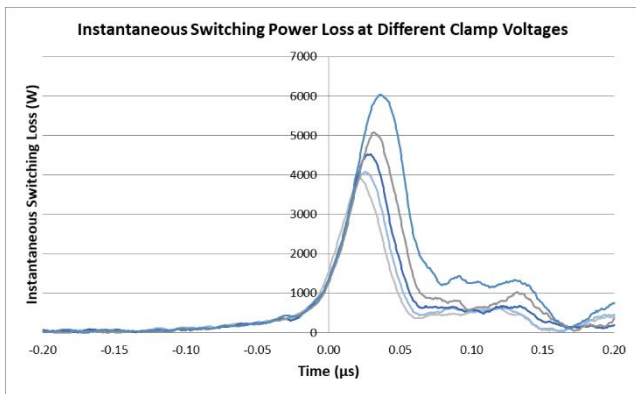


Fig. 10 (c) Switching loss dependence on clamping voltage.

Fig. 11 presents a summary of all losses in the circuit and shows how they are affected by the clamp voltage. The primary side conduction losses are significantly less than those in the secondary side due to there being significantly more current in the secondary and the primary duty ratio being only 15%. The switching loss on the primary side increases by 15 W (or 5% of input power) when the clamp voltage set-point increases from 210 V to 385 V, while the conduction losses show minimal decrease. The switching losses therefore dominate the overall efficiency. The more efficient modes of operation therefore occur at lower clamp voltages.

The losses shown in Fig. 11 however, do not account for the losses within the clamp itself. A lower clamp voltage set-point means a higher current flow through the clamp. This introduces additional losses as the clamp switch will also have switching and conduction losses. Even without this data a comparison can be made.

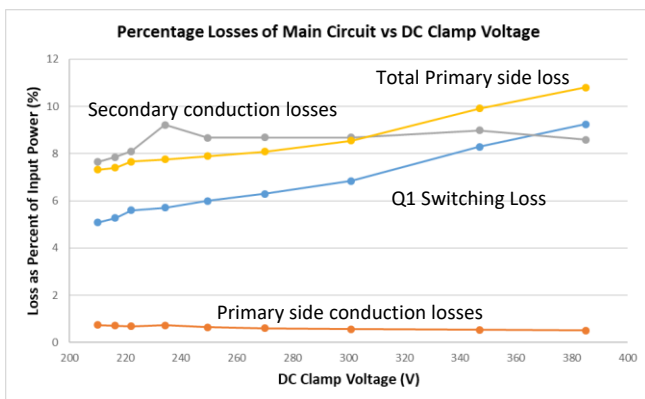


Fig. 11 Summary of switching and conduction losses.

C. Results Comparison

As the asymmetric half-bridge converter only has a fixed voltage across the coupled inductor to create a fair comparison of its efficiency, Fig. 2, to the voltage clamp single-ended coupled-inductor converter, Fig. 4, the same supply voltage of 150V as used creates a 300V potential difference across the coupled inductor. This then can be fairly compared to a 300V buck clamp voltage. The asymmetric half-bridge main switches (Q1 and Q2) are rated to at least V_{in} , whereas switch ratings of at least $V_{in}+VC2$ are required for the single-ended converter. This advantage of the asymmetric half-bridge was not utilized in these tests as the same devices were used for both to enable a fair comparison of the losses.

As shown in Fig. 12, for a 300V inductor potential difference, the asymmetric half-bridge offers higher efficiencies. The comparison between both converters does not account for the losses in clamp switch Q2. These losses could however become significant at lower clamp voltages due to the increase in clamp current flowing, and if they were included in the comparison the clamp circuit efficiency would be further reduced. The comparison at 300V therefore shows that the asymmetric half-bridge circuit offers better efficiency and lower rated devices.

Fig. 12 also shows that the clamp circuit efficiency is higher for clamp voltages of 210V and 216V. At these lower clamp voltages however it is likely that the clamp losses, which are neglected here, would be proportionally greater due to higher clamp current. Additionally, the comparatively lower rated MOSFET devices that can be deployed in the asymmetrical half-bridge converter offer lower conduction losses. In combination, these two effects suggest that the asymmetrical half-bridge converter will exhibit an efficiency advantage under all operating conditions.

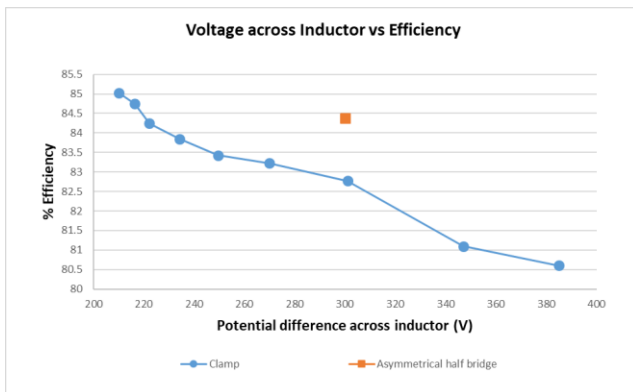


Fig. 12 Asymmetrical half-bridge and single-ended voltage clamped, coupled-inductor converter efficiencies versus inductor potential difference.

The asymmetric half-bridge requires no additional control to operate, as the additional switch is controlled by the same gate signal as switch Q1 although an isolated gate driver is required for Q2.

A further benefit of the asymmetric half-bridge is that the four power devices in the bridge only need to be rated at V_{in} whereas in the clamp both switches and additional diodes should be rated above the clamp voltage ($V_{in} + V_{C2}$). The asymmetrical half-bridge coupled-inductor converter utilizes diode clamping to protect the switches and create the required voltage across the coupled inductor.

A desalination plant would be powered by a rectified three-phase AC supply creating a DC supply voltage V_{in} of just under 600V. The asymmetrical half-bridge converter can therefore utilize 800V devices whereas the single-ended converter would require 1200V, or even 1700V, rated devices.

VII. CONCLUSION

A novel asymmetric half-bridge coupled-inductor buck converter circuit was compared with a single-ended coupled-inductor buck converter with a voltage clamp. The results presented show that the asymmetrical half-bridge converter provides an efficient circuit to drive the coupled-inductor buck converter. The leakage energy of the primary winding was managed within the bridge avoiding the need for a snubber circuit. Both switches are rated at just above the input supply voltage. Using the asymmetrical half-bridge to drive a coupled-inductor buck converter requires only one control signal as both switches on the primary side are switched simultaneously.

The single-switch coupled-inductor converter has the benefit of a single switch in the main forward path but needs an additional clamp circuit to control the voltage induced by the leakage inductance of the coupled inductor. This introduces the comparative disadvantage of requiring separate control for the duty cycle of the clamp switch.

Whilst the investigation has shown that lower clamp voltages can offer an efficiency advantage when compared to the asymmetric half-bridge circuit, full consideration of the clamp losses together with the efficiency advantages offered by lower rated MOSFET devices suggest that the asymmetric half-bridge circuit will always exhibit better efficiency. In the desalination application, the high turns ratio between primary and secondary increases the leakage inductance. The asymmetric half-bridge offers the most robust solution and highest efficiency because the leakage energy is recovered, and the switch voltages are clamped to within the voltage rating of the bridge.

REFERENCES

- [1] F. A. AlMarzooqi, A. A. Al Ghaferi, I. Saadat and N. Hilal. "Application of capacitive deionisation in water desalination: A review," *Desalination*, vol. 342, pp. 3–15, 2014.
- [2] T. J. Welgemoed and C. F. Schutte. "Capacitive deionization technology™: An alternative desalination solution," *Desalination*, vol. 183, no. 1–3, pp. 327–340, 2005.
- [3] R. C. Pollock, N. McNeill, D. Holliday and B. W. Williams. "DC-DC converter with a high step-down ratio for water desalination applications," in *IET PEMD Power Electronics Machines & Drives*, Liverpool, pp. 1-6, 2018.
- [4] T. Chen, S. Member, C. Chen and S. Member. "Characterization of asymmetrical half bridge flyback converter," in *IEEE 33rd Annual IEEE Power Electronics Specialists Conference.*, 2002, vol. IEEE 33rd, pp. 1–6.
- [5] D. Skendzic. "Two transistor flyback converter design for EMI control," in *IEEE International Symposium on Electromagnetic Compatibility*, .21-23 Aug, 1990, pp.130-133.
- [6] M. A. Pagliosa, T. B. Lazzarin and I. Barbi. "Output

- characteristics of two-switch flyback including the leakage inductance,” in 2015 IEEE 13th Brazilian Power Electronics Conference and 1st Southern Power Electronics Conference (COBEP/SPEC), 2015, no. 13th, pp.1-5.
- [7] T. Wu, T. Chen, Y. Chang and C. Chang. “Bi-directional converter with buck/forward active clamp,” in International Conference on Power Electronics and Drive Systems (PEDS), 2009, pp.1-6.
- [8] A. Ferraro. “An overview of low-loss snubber technology for transistor converters,” in 1982 IEEE Power Electronics Specialists conference, 1982, pp.466-477.
- [9] S. J. Finney, B. W. Williams and T. C. Green. “RCD snubber revisited,” IEEE Trans. Ind. Appl., vol. 32, no. 1, pp. 155–160, 1996.

Study of Site Location and Pipeline Routing for Future Natural Gas Importing Terminal Project in Morocco

¹Mahmoud Akdi, ²Firdaous El Ghazi, ³Moulay Brahim Sedra

¹Simolab, Ibn Tofail University, Kenitra, Morocco,

²Simolab, Ibn Tofail University, Kenitra, Morocco,

³Fste, UMI Moulay Ismail University of Meknes, Morocco,

¹makerase@gmail.com, ²elghazi.firdaous@gmail.com, ³mypedra@yahoo.fr

Abstract - In order to achieve sustainable supply combustible development, Morocco is projecting to invest in its first natural gas importing and storage capacity by 2030. This future project should be designed for electric power plants and other sectors using energy. It is not worthy that up today most of the existing power plants in Morocco are depending on coal in their electricity production, this is in contrast with the recent government environmental commitments.

Therefore, the aim of this article is to develop a research analysis related to the natural gas future project by introducing the main key aspects of choosing a site location and proposing an optimum routing for pipelines based on mathematic algorithms. It is proved that the port of Jorf Lasfar is a suitable importing terminal choice for Morocco. Afterwards, a pipeline routing will be proposed given the natural gas potential consumers. Thereby, the optimum pipeline routing starting from the importing terminal and linking the furthest consuming point is estimated at 490 Km.

Keywords - Dijkstra Algorithm, Financial preview, Natural gas, Nigeria - Morocco pipeline project, Operational research, Pipeline optimum routing.

I. INTRODUCTION

Facing major energy challenges, Morocco is increasingly orienting its strategic decisions towards reducing the use of polluting energy based on fossil sources. The global economic context presents significant development opportunities of Liquid Natural Gas (LNG) becoming an accessible energy source that is environment friendly and less expensive than other fuel-based or coal-based energies with a more important calorific value [1].

This global context presents a long-term opportunity for Morocco to develop electricity production and heavy industry plants that currently run on other polluting fuels. Therefore, Morocco has set itself the goal of achieving the first LNG import and storage

terminal in the Kingdom. The Ministry of Energy, Mines and Sustainable Development has confirmed the future investment, the import terminal should be designed to equip Morocco with the capacity to import, store and supply natural gas to the Gas To Power (GTP) and Gas To Industry (GTI) [2] sectors covered by this program.

Therefore, this article aims to develop a scientific approach for:

- Identification and choice of the importing site through a scoring system based on factual criteria;
- As part of the future Nigeria - Morocco pipeline project, proposal of the optimal routing based on the Dijkstra Algorithm;
- Tentative of a financial preview analysis.

This article deals with a current topic of natural gas development opportunities in Morocco, the analysis conclusion can significantly contribute to a decision making regarding the choice of the new LNG importing terminal location and the pipeline routing. The introduction of natural gas can definitely reduce the use of other polluting energy sources in the kingdom.

II. CHOICE OF LNG IMPORTING SITE LOCATION

For any investment project, the selection of the site location weighs heavily in the investment decision in the importing terminal. Choosing the best site location can significantly impact the profitability of a project and its future development. At the present time, there are three potential site locations choices that can host the LNG import terminal project, these sites are:

- Jorf Lasfar port site
- Kenitra port site « As Is »
- Kenitra new port « To Be »

A benchmark of the three sites is achieved below based on factual criteria. Afterwards, a comparison of the three sites is summarized through a scoring system considering the features of each site location [4].

1. Benchmark of the Potential Site Locations

A. Jorf Lasfar (Location: 33°7'N-8°38'O)

The port of Jorf Lasfar was built in 1975 to basically export raw phosphate produced by the Cherifian Office of Phosphate (OCP) industrial group. The development of the industrial area has contributed to the development of the port and gradually supply the petrochemical companies as well. In 2011, an extension of the port was carried out to ensure the reception of oil tankers and phosphatic products.

The port of Jorf Lasfar is served via the A1 highway and the regional road R306, as well as the national road N1 from El Jadida and from Safi via R316. A freight railroad line is also connected to the port. Jorf Lasfar is considered one of the most important ports in Morocco, its capacity is expanding to handle more traffic in the future. The evolution of the ports traffic is represented in Figure 1.

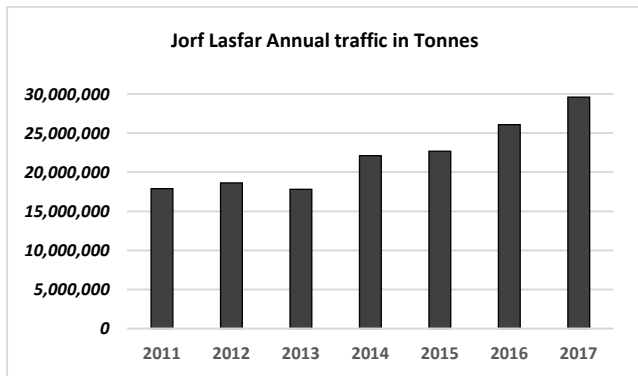


Fig .1 Jorf Lasfar port traffic evolution [3].

Figure 1 shows that the port ensures the reception of oil tankers and phosphatic products up to 30 000 000 tonnes in 2017.

As for the Jorf Lasfar port connectivity, the researchers present in Figure 2 a full description of the existing facilities.

The design of Jorf Lasfar port and the diversity of products crossing through have enhanced this port expertise in the reception of large cargoes. This site has several more advantages, including:



1	Dock at -15,6 m for phosphates.
2	Dock at -12,50 m for fertilizers.
3	Dock at -12,5 m for coal.
4 & 5	Dock at -12,5 m for sulfur.
6 & 7	Dock at -11,5 m for ammoniac.
8	Dock at -15,6 m for petroleum products.
9	Dock at -12,5 m for oil and gas.
10	Dock at -12,50 m for various products.
11	Dock at -9,5 m for various products.
12	Dock at -5 m for various products.
13	Dock at -5,25 m for various products.
14	Dock at -4 m for various products.
15	Dock at -2,5 à -3,5 m.
16	Dock at -12,5 m.

Fig .2 Jorf Lasfar port characteristics and connectivity.

- Access to the sea with a minimum water depth of 12 m at low tide for large transport vessels;
- Appropriate surface conditions for the development and extension installation that can accommodate other products;
- Proximity from power plants Jorf Lasfar Energy Company (JLEC) unit 1-2, unit 3-4 and unit 5-6 and OCP power plants;
- Possibility of installing the required LNG landing dock near the actual terminal site;
- Reasonable distance to install the LNG transfer lines from the unloading dock to the LNG storage tanks.

B. Kenitra “As Is” (Location: 34°16’N-006°41’O)

The port of Kenitra was built in 1912 for political and commercial reasons by the French protectorate in order to neutralize the competitive attraction of the port of Tangier. In 1996, the National Ports Agency (NPA) carried out development works to increase the river's hydraulic power and allow larger ships to access the wharves.

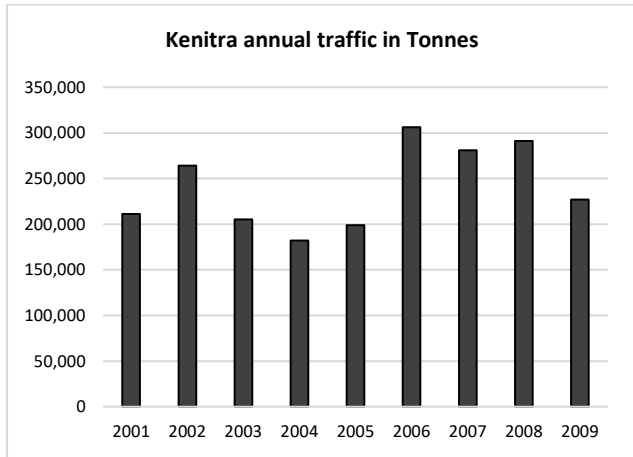


Fig .3 Kenitra port traffic evolution [3].

The evolution of traffic is represented in Figure 3.

As for the Kenitra port connectivity, the researchers present in Figure 4 a full description from the NPA official newsletter.

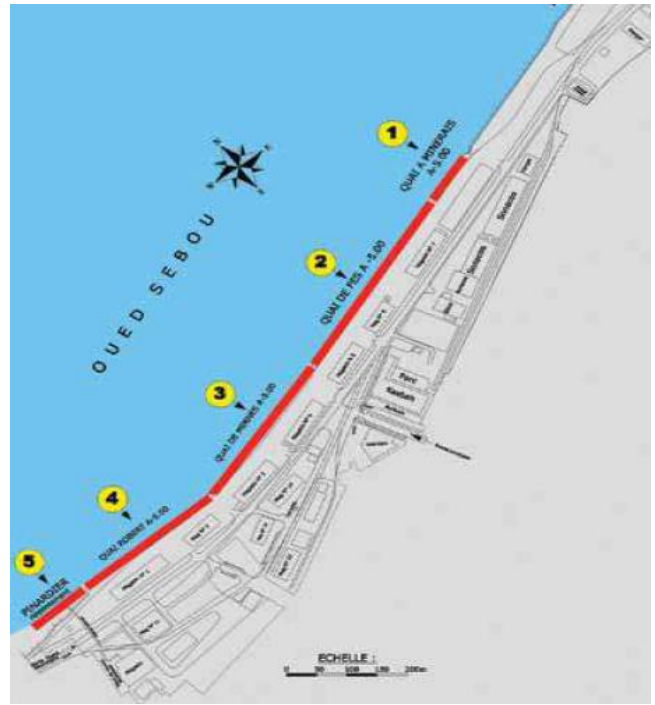
The current port has several limitations due to the crossing of Oued Sebbou river, the removal of the port of Kenitra to a new site nearby is being considered by the government. The new location will be the region of Oulad Bel Assal, at 24 km from Oued Sebou.

C. Kenitra “As Is” (Location: 34°16’N-006°41’O)

This new location of the port should bring the answers to the current limits of the Kenitra port by moving it to another location that remains nearby at 24 km at the north, and is even more accessible. This new port has the following advantages:

- Availability of land required for the construction of the new port (approximately 2000 Ha).
- Being located far away from the urban areas, this new location guarantees therefore the possibility of future extension.

Figure 5 shows the preliminary shaping of this port.



1	Dock at -5.00 m / zh with a length of 224 ml.
2	Dock at -5.00 m / zh; with a length of 246 ml.
3	Dock at -5.00 m / zh with a length of 300 ml.
4	Dock at -5.00 m / zh with a length of 100 ml.
5	Dock at -5.00 m / zh with a length of 60 ml.

Fig .4 Kenitra Port characteristics and connectivity.

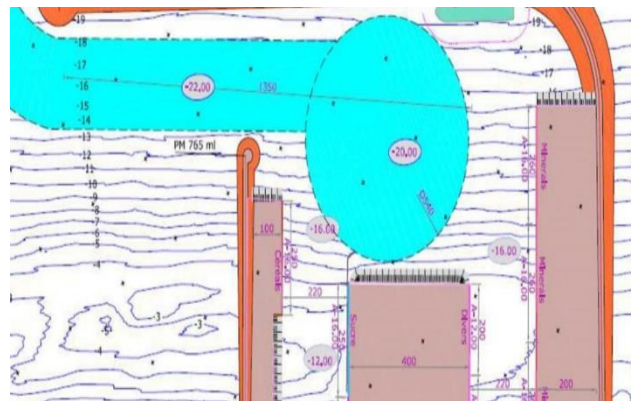


Fig .5 Evaluation study of the new Kenitra Atlantic port by Catram consulting [5].

The vocation of this new port is currently commercial as it will support the development of Kenitra city in terms of automotive industry for export as well as the reduction of traffic at Casablanca port that is already saturated.

The disadvantage remains relative to the investment required for this new port, estimated at 5 billion MAD [6]. This investment will be added to the investment required for the construction of the LNG import terminal and pipeline routing estimated at 45 billion MAD [7].

2. Site Selection Criteria

Referring to feedback from other similar LNG logistics platform projects [8], below are the main factors determining the choice of the appropriate import terminal location:

- Proximity of end use points and LNG future consumption sites;
- Proximity of the new pipeline project coming from Nigeria;
- Easy access and departure for LNG cargos,
- Distance from population areas;
- Conformity and extent of the land (available area, soil quality, geographical and topographical features, existence of groundwater tables);

- Ability to accommodate a future extension;
- Weather conditions;
- Exposure to natural hazards (earthquakes, plate tectonics, high tidal risk or potential tsunami hazards);
- Sensitivity of the surrounding environment (to be confirmed via environmental impact studies);

By using a scoring system from 1 to 5 for each criterion, the table below shows the comparison analysis between Kenitra port "As is", North Atlantic Kenitra Port (NAKP) "To Be" and Jorf Lasfar location. The ratings being:

- 1- Not Filled
- 2- Partially Filled
- 3- Half Filled
- 4- Satisfactory

Table 1. Comparison analysis between site locations.

	Jorf Lasfar	Kenitra "As is"	NAKP "To Be"	Comments
Proximity of end use points and LNG consumption sites	3	4	4	- The main consumption points are located in North West Morocco - The significant industrial areas remain half path between different ports.
Proximity of the new pipeline project coming from Nigeria	5	4	4	The situation of the port of Jorf Lasfar further south allows more proximity of connection with the future pipeline connecting Nigeria to Morocco.
Easy access and departure for LNG cargos	5	1	4	- The present port "As Is" of Kenitra has a difficult access for large boats, because of the passage by a parcel of Sebou river, additional investments are needed for site redevelopment. - The ease of access to the NAKP port is to be confirmed
Security distance available away from population areas	5	1	5	- The Jorf Lasfar area is classified an industrial area to be and located outside the urban perimeter. - Same as for the NAKP port "To Be"
Conformity and extent of the land	5	2	5	- Only the port of Kenitra "As Is" is limited in terms of possibility of extension.
Ability to accommodate a future extension	2	1	5	- Availability of land in NAKP port "To Be" is estimated at 2000 Ha.
Weather conditions	5	5	5	The weather is favorable in all locations.
Exposure to natural hazards	4	5	4	Unlikely risk, close exposure level for all location.
New investments necessary to accomodate the port site	5	4	1	- The new NAKP port "To Be" is in its study phase, the planned investment is 5 billion MAD. - Kenitra port "As Is" requires investment to allow LNG cargoes to pass through. - Only the port of Jorf Lasfar is currently adapted and ready to receive an import terminal.
Final Scoring	39	27	37	

Jorf Lasfar port and NAKP "To Be" locations have the best yet close final scoring.

Figure 6 represents the comparison result between the three possible locations.

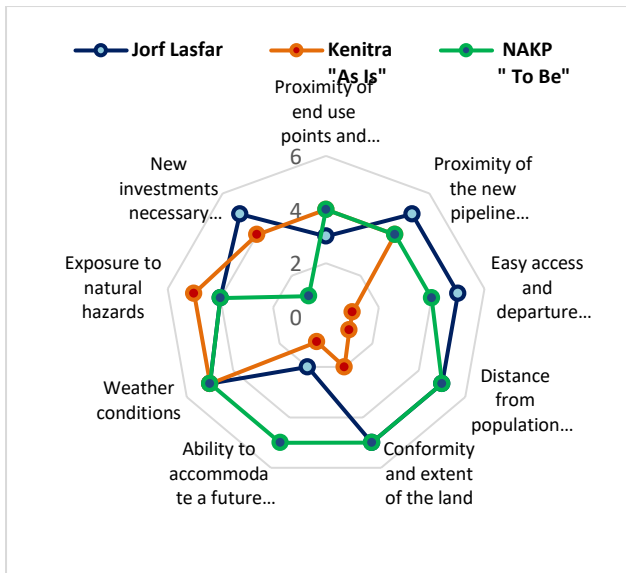


Fig .6 Final scoring of each potential site choice.

In general, since it is difficult to meet all the optimal conditions on a single location, some requirements can be reached by making changes on site at a relatively acceptable cost, the feedback from several similar projects indicates that the key variable that is likely to be discriminatory is the depth of the maritime jetty: if the depth of the water is not sufficient, the cost of carrying out development work increases and several technical constraints of reception process will be considered.

After careful considerations, the Jorf Lasfar location and the NKAP "To Be" seem both to be suitable locations for the future LNG terminal. These two locations have more many advantages when compared to Kenitra "As Is" location. However, Jorf Lasfar location, being already an existing operating port, and the NPKA" To Be" being a future port requiring an important construction budget, it is more cautious to select the Jorf Lasfar location if no further new data are revealed in the future.

The Jorf Lasfar site presents the favorable geographic location and it the best location that meets the selection criteria. It represents the least expensive site in terms of new redevelopment investments and represents fewer uncertainties in terms of costs and deadlines. This port will have the capacity to meet the national LNG import need for seizing future development opportunities.

III. PIPELINE OPTIMUM ROUTING

1. LNG Future Consumers

The import terminal project is intended to meet the needs of the country regarding LNG energy needed for the GTP and GTI programs. The investment in pipeline routing is equally important as the investment in the terminal construction itself.

It's clear that finding the optimum pipeline routing shall improve the profitability of this investment project. The first step is to find out the different consuming points and their locations, then classify the planned connection points for the pipeline as follows.

A. Electricity power plants

The power plants concerned, also called Combined Cycle Gas Turbine (CCGT), will have a percentage of electricity to be produced from natural gas. In order to do so, investments are planned to adapt the existing production facilities.

The power plants concerned are listed below [9].

Table 2. Power plants locations.

Power plant name	City/Region	Capacity in MW
CCGT Kenitra	Kenitra	450 MW
CCGT Mohammedia	Mohammedia	450 MW
AL Wahda	Sidi Kacem city	2 x 600 MW
Dhar Doum	120 km south to Tangier	2 x 600 MW
Oued Al Makhazine	100 km south to Tangier	2 x 600 MW
Tahhadart	Tahhadart Region	MW

B. Industrial areas and natural gas discovered basins

The pipeline routing should be able to cross a large industrial area, known to be host to many energy consuming industries, such as the ceramics industry and other heavy industries located in Casablanca – Settat Industrial area.

On the other hand, there are two natural gas discovered basins: the underground basin of Sidi Yahya Lgharb and the underground basin of Tendrara. It's preferable that the natural gas pipeline shall be able to cross the discovered natural gas basins.

C. Existing and future LNG pipelines

The pipeline routing should be able to cross a large industrial area, known to be host to many energy consuming industries, such as the ceramics industry and other heavy industries located in Casablanca – Settat Industrial area.

- Existing Gazoduc Maghreb Europe (GME) pipeline: It is the Maghreb Europe Pipeline, which starts from Algeria, goes through northern Morocco, crosses the Gibraltar and joins Spain. Its diameter is 48 inches, its total length is 1300 km, including 45 km offshore and 540 km onshore on Moroccan soil.
- Future Nigeria - Morocco pipeline: This megaproject is part of a development policy in Africa, a cooperation agreement was signed between Nigeria and Morocco in December 2016. Currently, the study of this project is in FEED (Front END and Engineering Design) phase [10]. For Several economic and political reasons, the routing of the pipeline will be operated on a combined onshore / offshore routing, the estimated length of the pipeline will be about 5.700 km. It should be noted that investment estimates are still being revised by engineering studies. The pipeline routing can be settled after signing and negotiating access rights. Currently, this pipeline will serve many countries such as Benin, Togo, Ghana, Liberia, Sierra Leone, Guinea, Guinea Bissau, Gambia, Senegal and Mauritania before arriving to Morocco.



Fig .7 Planned pipeline routing, from the official website Lesinfos.ma.

In summary, the optimal pipeline routing shall be carefully designed to best meet consumption expectations, this pipeline must meet the following requirements:

- Being carried out in the continuity of the pipeline from Nigeria, this pipeline will arrive to Morocco

- through several countries in northwestern Africa and passing through Senegal.
- Powering the combined cycle power plants concerned by the GTP investment plan.
- Meeting the GTI need via a passage through the most important industrial area.
- The pipeline routing should take the shortest possible distance.
- The Optimum routing shall confirm the best choice of the new importing terminal.

This is an optimization problematic of the pipeline routing. The researchers present their input data and working assumptions in the form of a short-run operational search problem, Dijkstra algorithm is suitable to solve it.

2. Dijkstra Algorithm

Dijkstra algorithm [11] is known to be one of the most effective operational search algorithms for tracing the shortest path between multiple two distant starting and arriving points, including many intermediary possible stops and constraints. Also called graph theory, this algorithm was invented by the Dutch researcher Edsger Dijkstra in 1959. Among the most common applications of this algorithm are the telecommunications networks and the supply chain traffic.

The principle is to express the problem in the form of a graph with nodes that symbolize the intermediate stopping points, the edges symbolize the path in km between two successive nodes.

We note the graph $G = \{ N ; U_{ij} \}$

We classify the nodes into 5 categories as follows:

Table 3. Nodes classification.

Departure node	
α	Nigeria
Intermediary node	
β	Senegal
Possible locations for LNG terminal	
X	Jorf Lasfar
Y	NAKP "To Be"
Power stations crossing points	
A	Mohammedia Power Station
B	Kenitra Power Station
C	Al Wahda Power Station
D	Dhar Doum Power Station
E	Oued Al Makhazine Power Station
F	Tahhadart Power Station

Other crossing points	
A	Casablanca – Settat Industrial Zone
B	Underground basin of Sidi Yahya Lgharb
C	Gazoduc Maghreb Europe
D	Underground basin of TENDRARA

Therefore, our Dijkstra graph is composed of 14 nodes:

$$N = \{\alpha; \beta; X; Y; A; B; C; D; E; F; a; b; c; d\}$$

The researchers consider the following assumptions:

- The pipeline routing from the import terminal should be linked with the pipeline coming from Nigeria.
- The graph will contain two possible nodes for the import terminal, the algorithm will define the most ideal location to respect the shortest pipeline path.
- In terms of LNG consumption points, only CCGT power plants included in the GTP investment program are considered the most important crossing points.
- the underground natural gas basins are optional crossing points since the main natural gas resource will be imported by the future LNG terminal.

$U(i;j)$ represents the set of distances between two nodes i and j ; therefore:

$$\begin{cases} U(\alpha; \beta) = 4000 \text{ km} \\ U(\beta; X) = 2400 \text{ km} \\ U(\beta; Y) = 2700 \text{ km} \end{cases}$$

$$\begin{cases} U(X; a) = 114 \text{ km} \\ U(Y; a) = 120 \text{ km} \\ U(Y; B) = 15 \text{ km} \\ U(a; B) = 115 \text{ km} \\ U(B; b) = 30 \text{ km} \\ U(a; b) = 140 \text{ km} \end{cases}$$

$$\begin{cases} U(X; A) = 130 \text{ km} \\ U(a; C) = 265 \text{ km} \\ U(b; C) = 60 \text{ km} \end{cases}$$

$$\begin{cases} U(b; D) = 90 \text{ km} \\ U(C; D) = 70 \text{ km} \\ U(D; c) = 5 \text{ km} \end{cases}$$

$$\begin{cases} U(c; d) = 110 \text{ km} \\ U(D; E) = 70 \text{ km} \end{cases}$$

$$\begin{cases} U(E; F) = 30 \text{ km} \\ U(C; D) = 70 \text{ km} \end{cases}$$

The distances are calculated between the nodes based on the Global Positioning System (GPS) geolocation on the map. The indicated distances do not consider some potential disturbance factors such as soil surveys, driving constraints or natural obstacles that may arise to deflect the proposed routing.

The problematic is represented in a graphic form in Figure 8, the nodes represent the potential crossing points of passage of LNG consumption, they are connected by arcs with the distance in km between the nodes.

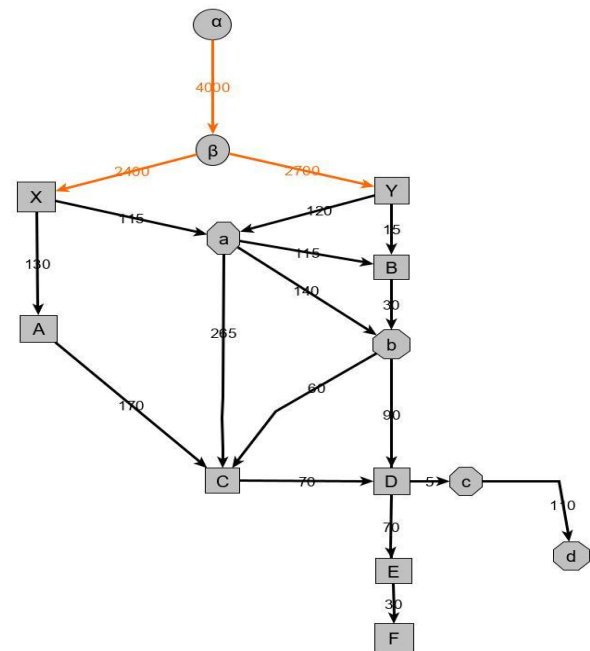


Fig .8 Dijkstra graphic representation.

$U(i,j)$ is the distance of the arc from i to j .

Starting from the top node α , $D[i]$ the distance of the shortest path found at a given step.

E is the set of nodes of passage composing the shortest definitive path. At first, E contains only the first node α , in each step, the next node is added to E and the distance $D[i]$ is updated.

Therefore, our Dijkstra algorithm can be expressed by the following function:

$$E = \{\alpha\}$$

For each node $\neq \alpha$, the researchers consider the following:

$$D[i] = U[\alpha; i]$$

The researchers consider $t \in E$ if $D[t]$ the minimum possible distance, then $E_t = E \cup \{t\}$;

For each:

$$i = [\beta; X; Y; A; B; C; D; E; F; a; b; c; d]$$

i is successor passage node to t if:

$$[D(t) + U(t; i)] < D(i)$$

Then, (3) $D(i) = D(t) + U(t; i)$ and $i \in E$

If not $i \notin E$

Therefore, the representation of the Dijkstra algorithm is as follows:

STEP	α	β	X	Y
1	0	4000	α	
2	χ	4000	4600β	6700β
3	χ	χ	4600β	
4	χ	χ	χ	
5	χ	χ	χ	
6	χ	χ	χ	
7	χ	χ	χ	
8	χ	χ	χ	6700β
9	χ	χ	χ	χ
10	χ	χ	χ	χ
11	χ	χ	χ	χ
12	χ	χ	χ	χ
13	χ	χ	χ	χ

STEP	A	B	C	D	E	F
1						
2						
3	6530	X				
4		6630/a	6780/a			
5	6530/X		6700/A			
6	χ	6630/a				
7	χ	χ	6720/b	6750/b		
8	χ	χ	6720/b	6790/C		
9	χ	χ	χ	6790/C	6860/D	
10	χ	χ	χ	χ		
11	χ	χ	χ	χ		
12	χ	χ	χ	χ	6860/D	6890/E
13	χ	χ	χ	χ	χ	6890/E

STEP	a	b	c	d
1				
2				
3	6515/X			
4	6515/X	6655/a		
5	χ			
6	χ	6660/B		
7	χ	6660/B		
8	χ	χ		
9	χ	χ	6795/D	
10	χ	χ	6795/D	6905/c
11	χ	χ	χ	6905/c
12	χ	χ	χ	χ
13	χ	χ	χ	χ

The interpretation of the result is done by following the step numbers and the nodes in bold and corresponding distances indicate the optimum routing.

Table 4. Optimum routing steps.

Step	t	D (t)	E
1	α	0	{ α }
2	β	4000	{ $\alpha; \beta$ }
3	X	6400	{ $\alpha; \beta; X$ }
4	a	6515	{ $\alpha; \beta; X; a$ }
5	B	6630	{ $\alpha; \beta; X; a; B$ }
6	b	6660	{ $\alpha; \beta; X; a; B; b$ }
7	C	6720	{ $\alpha; \beta; X; a; B; b; C$ }
8	D	6790	{ $\alpha; \beta; X; a; B; b; C; D$ }
9	E	6860	{ $\alpha; \beta; X; a; B; b; C; D; E$ }
10	F	6890	{ $\alpha; \beta; X; a; B; b; C; D; E; F$ }

The optimum distance from point α (Nigeria) to point F (Tahhadart power station) is 6 890 km.

Given the 6400 km between Nigeria and Jorf Lasfar, the shortest distance from Jorf Lasfar to power station Tahhadart is 6 890 km – 6 400 km = 490 km.

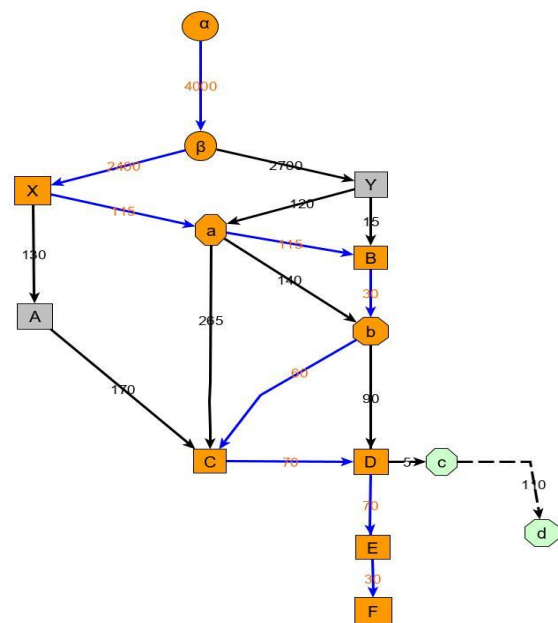


Fig .9 Dijkstra graphic solution.

The optimal routing given by Dijkstra algorithm goes through the following nodes marked in orange in Figure 9.

3. Results Interpretation

The optimum routing can be described as follows:

Table 5. Optimum routing description part 1.

Departure	α	Nigeria 4000 km
	β	Senegal 2400 km
LNG terminal	X	Jorf Lasfar Location 115 km
Industrial area	a	Settat - Casablanca 115 km
Power station 1	B	Kenitra power station 30 km
Underground basin 1	b	Sidi Yahya Lgharb basin 60 km
Power station 2	C	Al wahda power station 70 km
Power station 3	D	Dhar Doum power station 70 km
Power station 4	E	Oued al Makhazine power station 30 km
Power station 5	F	Tahhadart power station

A complementary routing can also be proposed to link the pipeline project with the existent GME pipeline, and then arrive to Tendirara Underground basin. Therefore, this complementary routing will be as follows:

Table 6. Optimum routing description part 2.

Power station 3	D	Dhar doum 5 km
GME gazoduc	c	Gazoduc Maghreb Europe 110 km
Underground basin 2	d	Tendirara basin

This study aims to achieve two main objectives; the first is to confirm the ideal location for LNG importation terminal and the second is to propose the shortest pipeline routing between the departure point α representing Nigeria and the arrival point F representing the Tahhadart power station.

The optimal routing is shown on the following map:

Using Dijkstra algorithm, the Jorf Lasfar site is also suggested to be a suitable choice location for the future import terminal port.

Starting the Jorf Lasfar port, the crossing points are: 5 power stations, 2 underground basins and 1 industrial area.

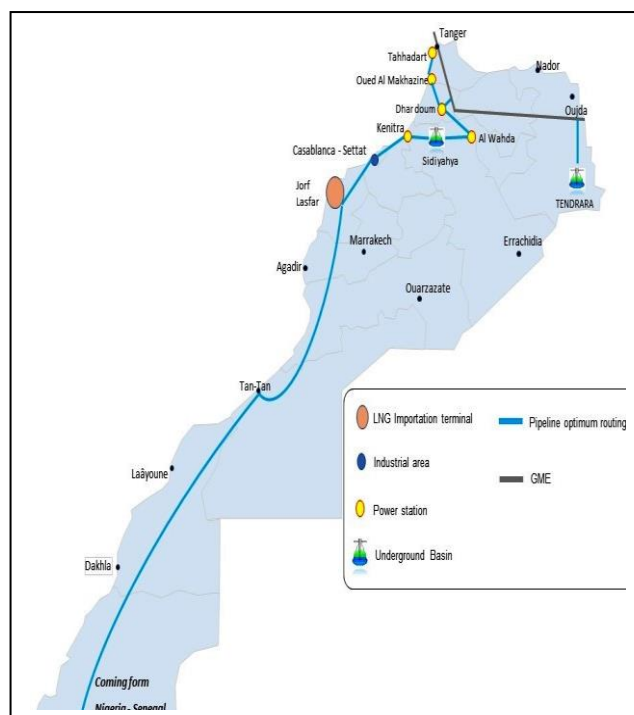


Fig .10 Optimum routing solution.

IV. FINANCIAL EVALUATION PREVIEW

After defining the pipeline shortest routing, the cost for the future pipeline is hard to evaluate given the available data at this moment. The cost of the pipeline can weigh heavily in the amount of the project investment, its cost depends on several unknown parameters such as the type and the diameter of the pipeline, the cost of the steel, the width of the pipeline, the nature of the environment and the depth of its passage.

The investment reference announced for 5660 km of the Nigeria - Morocco pipeline project is estimated at 20 to 50 billion dollars [11]. Therefore, considering the same pipeline characteristics for 490 km portion of pipeline proposed routing, the investment can be estimated at 1,8 to 4,5 billion dollars. This investment shall cover all the performances bellow:

- Engineering studies
- Execution study (works, cathodic protection ...)
- Civil engineering work
- Pipeline works
- Installation work of compression stations
- Piping and connection work

- Cathodic protection installation work
- Leak detection system installation work
- Pre-commissioning
- Commissioning

It's difficult to go any further in the rentability study since the international natural gas market is made up of different regional markets, making it difficult to talk about regular prices. Figure 11 can demonstrate the extreme volatility in natural gas prices.

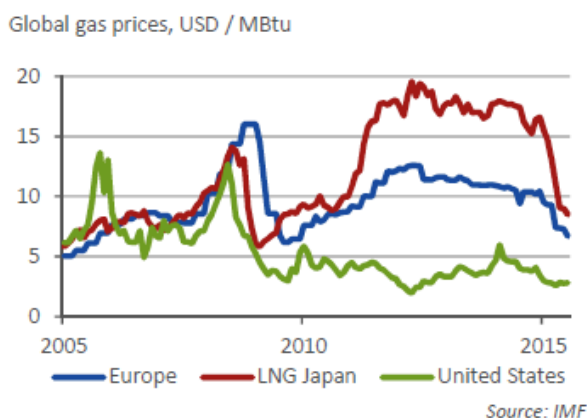


Fig .11 Gas prices volatility from the International Monetary Fund official newsletter.

The correlation between the price of oil and LNG is difficult to establish as these two markets are distinct. All LNG supply contracts are governed by a start date and an expiration date. During this period, the contract specifies the quantities supplied as well as the upper and lower tolerated variation limits.

In general, the main components of the price of natural gas are:

- The gas wellhead price
- The sea freight, and
- The cost of transportation along a distance

Price is governed by the strength of supply and demand, which can lead to price fluctuations as the market loses or regains its balance. To reduce its exposure to price volatility, significant storage capacity would be required to import and store the gas when prices are low often in summer when demand is lower. Many buyers also use financial assurance systems, such as hedging.

The rentability study of this project can be another interesting aspect to develop when more financial and contractual data about the project are revealed.

V. CONCLUSION

The Kingdom of Morocco has shown a growing preference for LNG to assure energy efficiency.

Given the significant international changes in energy supply and environmental protection, the new national energy strategy is progressively ensuring its procurement of natural gas while driving the energy transition with pragmatism and anticipation. In this context, this article developed two aspects of this program:

- The choice of site location for the LNG import, storage and regasification terminal
- The shortest path for distribution and connection pipeline using the Dijkstra algorithm

The pipeline routing is an important part of the LNG project in terms of necessary investment. This routing should adapt to many constraints of passage and come in continuity of the pipeline connecting Nigeria to Morocco.

The port of Jorf Lasfar is a suitable importing terminal choice. The pipeline perimeter supported by the national LNG project is identified between the import terminal and the furthest point of consumption, the pipeline routing starting from Jorf Lasfar terminal and linking the consumption points is estimated at 490 km.

The environmental qualities of natural gas largely justify the conduction of this project. With its high hydrogen content, gas combustion is considered perfect and does not produce heavy unburnt harmful particles for environment or health. Given the tax incentives and government conventions planned in Morocco to encourage the use of natural gas, the profitability of this investment is guaranteed on a long term.

REFERENCES

- [1] R. Laplante, F. L'Italien, N. Mousseau, and S. Labranche, 2nd International Summit Of Research Cooperatives In Community Development, Energy transition, how to get out from fossil fuel UNIVERSITY OF QUEBEC, available on: <http://normandmousseau.com/publications/159.pdf> [2015]

- [2] Amara, Ministry of Energy, Mines, Water and Environment, Roadmap of the National Development Plan for Liquefied Natural Gas. P. 11, available on: <https://fr.scribd.com/doc/250255788/Plan-National-Marocain-de-Developpement-Du-Gaz-Naturel-Liquefie-Gnl> [2014].
- [3] The National Ports Agency. Available on : <http://www.equipement.gov.ma/Carte-Region/RegionSafi/Patrimoine-des-infrastructures-regionales/Ports-maritimes/Pages/Fiche-Synthetique-Port-Jorf-Lasfar.aspx> [2019]
- [4] The National Ports Agency. Available on: <https://www.anp.org.ma/Services/Portkenitra/Pages/Presentation.aspx> [2019]
- [5] CATRAM Consulting, Evaluation Study of the New Kenitra Atlantic. Available on: <https://www.catramconsultants.com/kenitra-atlantique/> 2017
- [6] Official Announcement from the Management of the National Ports Agency. Available on: <http://fr.le360.ma/economie/anp-5-milliards-de-dirhams-dinvestissements-au-programme-111725> [2017]
- [7] Ministry of Energy, Mines, Water and Environment (2017). Draft Law Relating to the Downstream Sector of Natural Gas in Morocco. N° 9417, page 2.
- [8] R. Tarakad, LNG Receiving and Regasification Terminals, an Overview of Design, Operation and Project Development Consideration, pp. 31--34, [2003].
- [9] Amara , Ministry of Energy, Mines, Water and Environment, Roadmap of the National Development Plan for Liquefied Natural Gas. p. 7, available on: <https://fr.scribd.com/doc/250255788/Plan-National-Marocain-de-Developpement-Du-Gaz-Naturel-Liquefie-Gnl> [2014]
- [10] Benchmark of the Royal Institute of Strategic Studies , available on: <https://www.medias24.com/MAROC/ECONOMIE/ECONOMIE/188546-Gazoduc-Maroc-Nigeria-Voici-un-benchmark-de-l-Institut-royal-des-etudes-strategiques.html> [2018]
- [11] N.Jasika, and N.Alispaic . “Dijkstra's shortest path algorithm serial and parallel execution performance analysis,” INSPEC Accession Number: 12865637. Available on: <https://ieeexplore.ieee.org/abstract/document/6240942/figures#figures> [2012]



Scan the QR Code

Journal of
Renewable Energy and Sustainable
Development

RESD

Volume 5, Issue 1, June 2019 ISSN 2356-8569



ISSN 2356-8569

<http://apc.aast.edu>

